

1 **Functional analysis of *ESRP1/2* gene variants and *CTNND1* isoforms in orofacial**  
2 **cleft pathogenesis**

3  
4 Caroline Caetano da Silva<sup>1\*</sup>, Claudio Macias Trevino<sup>2\*</sup>, Jason Mitchell<sup>3\*</sup>, Hemma  
5 Murali<sup>8</sup>, Casey Tsimbal<sup>1,4</sup>, Eileen Dalessandro<sup>1</sup>, Shannon H. Carroll<sup>1,4</sup>, Simren  
6 Kochhar<sup>5</sup>, Sarah W. Curtis<sup>5</sup>, Ching Hsun Eric Cheng<sup>1</sup>, Feng Wang<sup>6</sup>, Eric Kutschera<sup>6</sup>,  
7 Russ P. Carstens<sup>7</sup>, Yi Xing<sup>6,8</sup>, Kai Wang<sup>8</sup>, Elizabeth J. Leslie<sup>5</sup>, and Eric C. Liao<sup>1,2,4,9,\*\*</sup>

8  
9 <sup>1</sup> Center for Craniofacial Innovation, Division of Plastic and Reconstructive Surgery,  
10 Department of Surgery, Children's Hospital of Philadelphia, PA, USA  
11 <sup>2</sup> Harvard Medical School, Boston, MA, USA  
12 <sup>3</sup> Massachusetts General Hospital, Boston, MA, USA  
13 <sup>4</sup> Shriners Hospital for Children, Tampa, FL, USA  
14 <sup>5</sup> Department of Human Genetics, Emory University School of Medicine, Atlanta, GA,  
15 USA  
16 <sup>6</sup> Center for Genomic Medicine, Department of Biomedical and Health Informatics,  
17 Children's Hospital of Philadelphia, PA, USA  
18 <sup>7</sup> Department of Medicine, University of Pennsylvania Perelman School of Medicine,  
19 Philadelphia, PA, USA  
20 <sup>8</sup> Department of Pathology and Laboratory Medicine, University of Pennsylvania  
21 Perelman School of Medicine, Philadelphia, PA, USA  
22 <sup>9</sup> Department of Surgery, University of Pennsylvania Perelman School of Medicine,  
23 Philadelphia, PA, USA  
24

25 \* These authors contributed equally to the work

26 \*\* Corresponding author

27

28 Eric C. Liao, MD, PhD  
29 Director, Center for Craniofacial Innovation  
30 Surgery Vice Chair of Academic Affairs, Children's Hospital of Philadelphia  
31 Professor of Surgery, University of Pennsylvania Perelman School of Medicine

32

33 CTRB 11006  
34 3501 Civic Center Blvd.  
35 Philadelphia, PA 19104  
36 liaoce@chop.edu

37 **Abstract**

38 Orofacial cleft (OFC) is a common human congenital anomaly. Epithelial-specific RNA  
39 splicing regulators *ESRP1* and *ESRP2* regulate craniofacial morphogenesis and their  
40 disruption result in OFC in zebrafish, mouse and humans. Using *esrp1/2* mutant  
41 zebrafish and murine Py2T cell line models, we functionally tested the pathogenicity of  
42 human *ESRP1/2* gene variants. We found that many variants predicted by *in silico*  
43 methods to be pathogenic were functionally benign. *Esrp1* also regulates the alternative  
44 splicing of *Ctnnd1* and these genes are co-expressed in the embryonic and oral  
45 epithelium. In fact, over-expression of *ctnnd1* is sufficient to rescue morphogenesis of  
46 epithelial-derived structures in *esrp1/2* zebrafish mutants. Additionally, we identified 13  
47 *CTNND1* variants from genome sequencing of OFC cohorts, confirming *CTNND1* as a  
48 key gene in human OFC. This work highlights the importance of functional assessment  
49 of human gene variants and demonstrates the critical requirement of *Esrp-Ctnnd1*  
50 acting in the embryonic epithelium to regulate palatogenesis.

51

52

53

54

55

56

57

## 58 Introduction

59 The study of orofacial cleft (OFC) has been foundational to genetic analysis of  
60 congenital anomalies. Craniofacial structural malformations are amenable to detailed  
61 phenotypic classification in large cohorts where genomic studies have been carried out  
62 to identify associated loci (1-8). As whole-genome sequencing (WGS) strategies and  
63 technologies advance, a growing list of genes and gene variants associated with OFC  
64 are being cataloged (1, 8-11). These approaches have uncovered the critical role of  
65 many genes regulating the embryonic oral epithelium in palate formation and OFC  
66 pathogenesis, including: *TP63*, *IRF6*, *GRHL3*, *ESRP1/2*, *CTNND1* (12-24).

67 Because most cases of non-syndromic OFC occur sporadically, the pathogenicity  
68 of variants cannot be inferred or supported by segregation among affected family  
69 members. Therefore, determining the functional significance of gene variants remains  
70 challenging. Multiple *in silico* predictive algorithms such as SIFT, PolyPhen-2,  
71 MutationTaster, PROVEAN and AlphaMissense offer functional predictions for gene  
72 variants utilizing amino acid sequence information, sequence conservation, biophysical  
73 properties, or homolog alignment (25-30). However, when given the same gene  
74 variants, these predictive tools may provide null values or contradicting results (31, 32).  
75 Indeed, the American College of Medical Genetics and Genomics and the Association  
76 for Molecular Pathology (ACMG-AMP), weights functional studies higher than *in silico*  
77 evidence for asserting pathogenic potential in gene variants for genes not previously  
78 established as causal for a particular disease (33-35). We and others previously  
79 showed that functional testing of human gene variants is essential, as *in silico*  
80 approaches alone fail to reach the necessary accuracy for clinical translation (36-40).

81 While bioinformatics tools have greatly facilitated the functional interpretation of genetic  
82 variants (41-43), it is also important to note the essential role of functional validation of  
83 gene variants, especially for those genes where computational predictions tend to differ  
84 from experimental validation (44-50).

85 *ESRP1* and its paralog *ESRP2* are epithelial splicing regulatory proteins that co-  
86 localize with *Irf6* and function in the embryonic epithelium to regulate craniofacial  
87 development and epithelial-mesenchymal transition during embryogenesis (22, 51-53).  
88 Global transcriptome analysis comparing mutant *irf6* and wildtype zebrafish revealed  
89 that the epithelial-specific splicing regulator *Esrp1* was differentially expressed (52). We  
90 showed that *Esrp1* and *Esrp2* are colocalized in the periderm and oral epithelium and  
91 are required for the formation of the anterior neurocranium (ANC), a teleost embryonic  
92 structure developmentally analogous to the mammalian primary palate in the manner  
93 that it is formed from the convergence of frontonasal derived midline prominence and  
94 paired maxillary projections (54-57). Targeted disruption of *Esrp1* in the mouse resulted  
95 in bilateral cleft lip and palate (21). In the *esrp1/2* double homozygote zebrafish, cleft  
96 formed in the ANC and extended to the upper edge of the mouth opening, analogous to  
97 the cleft lip and/or palate (CL/P) phenotype observed in the *Esrp1/2* mutant mice (22,  
98 52). In humans biallelic *ESRP1* mutations were described to cause hearing loss (58),  
99 heterozygous *ESRP2* mutations were associated with CL/P (20) and both *ESRP1* and  
100 *ESRP2* splicing targets were related to cancer-associated processes (59). Given the  
101 central role of *ESRP1* in periderm and embryonic epithelial development, there is likely  
102 selection against deleterious *ESRP1* alleles so that variants associated with hearing

103 deficit are likely hypomorphic and homozygous or biallelic loss-of-function alleles are  
104 likely embryonic lethal and not observed clinically.

105         Here, we applied complementary *in vivo* and *in vitro* models to functionally  
106 interrogate human *ESRP1* and *ESRP2* gene variants. To increase the rigor of the  
107 functional test using another independent assay, we also examined *Esrp*-mediated  
108 alternative splicing in a murine *Esrp1/2* double knockout Py2T cell model. The Py2T cell  
109 line has been used effectively to study epithelial mesenchymal transition and we have  
110 previously generated and characterized *Esrp1* and *Esrp2* double knock-out Py2T lines  
111 (23, 53). Using these independent approaches, we functionally determined the  
112 pathogenicity of the 7 *ESRP1* and 12 *ESRP2* human gene variants from CL/P cohorts  
113 or reported in hearing loss. We previously showed that *Esrp1/2* regulated splicing of  
114 *Ctnnd1* (60). Using RNAscope, we found that *Ctnnd1* transcripts co-localized with *Esrp1*  
115 and *Esrp2* in the mouse and zebrafish embryonic oral epithelium. The *esrp1/2* zebrafish  
116 model also presented a functional assay to test the function of *Esrp*-regulated genes  
117 such as *Ctnnd1*. In fact, exogenous expression of *ctnnd1* mRNA in zebrafish *esrp1/2*  
118 mutants partially rescued the cleft ANC, foreshortened pectoral fin and fused otolith  
119 phenotypes. Additionally, WGS of CL/P cohorts identified 13 new *CTNND1* gene  
120 variants, making this one of the most frequently associated genes in OFC. Taken  
121 together, these results demonstrate the critical requirement of *Esrp-Ctnnd1* operating in  
122 the embryonic epithelium to regulate palatogenesis.

123

## 124 **Methods**

### 125 Animal husbandry and breeding

126 Zebrafish (*Danio Rerio*) of the Tübingen strain were raised and bred following approved  
127 institutional protocols at Massachusetts General Hospital. Embryos were collected and  
128 raised in E3 Medium (5.0 mM NaCl, 0.17 mM KCl, 0.33 mM CaCl<sub>2</sub>, 0.33 mM MgSO<sub>4</sub>)  
129 containing 0.0001% Methylene blue at 28.5°C.

130

### 131 Gene variant identification, sequence alignment, and variant effect prediction

132 Three WGS datasets of 759 OFC trios from the Gabriella Miller Kids First (GMKF)  
133 Research (dbGaP; European trios, dbGaP: phs001168.v2.p2; Colombian trios, dbGaP:  
134 phs001420.v1.p1; Taiwanese trios, dbGaP: phs000094.v1.p1) were filtered for variants  
135 in *ESRP1*, *ESRP2*, and *CTNND1* that were (1) heterozygous in the affected patient, (2)  
136 had a minor allele frequency no greater than 0.001 in any population in gnomAD or  
137 1000 Genomes, and (3) had a variant consequence of missense, frameshift, stop-gain,  
138 splicing, or in-frame insertion/deletion. We further supplemented the resulting list with  
139 additional variants from ClinVar associated with an OFC or autosomal recessive  
140 deafness. In total, the ClinVar list included 12 *ESRP1* and 20 *ESRP2* variants. ClinVar  
141 variants were accessed in 2021, we note that new variants have been uploaded to  
142 ClinVar for *ESRP1* and *ESRP2*, but these new variants did not include relevant clinical  
143 phenotype information so were not included in this study. OFC associated genes were  
144 based on a previously published study that curated a list of approximately 500 genes  
145 based on known clinical syndromes and association results from GWAS (61).

146

147 To further refine the variant list to identify variants for testing in mouse and  
148 zebrafish assays, we aligned the human, mouse and zebrafish *Esrp1* and *Esrp2* amino  
149 acid sequences using Clustal Omega (62). 7 *ESRP1* and 12 *ESRP2* variants at fully  
150 conserved residues were then annotated using SIFT, PolyPhen-2, and AlphaMissense  
151 to obtain the predicted change in protein function and were categorized as benign,  
152 pathogenic, or of unknown significance. We included a silent mutation from *ESRP2*, at  
153 threonine 475 (T475T) that served as an internal negative control. Variants were  
154 annotated to the following human transcripts: *ESRP1*: NM\_017697.4/  
155 ENST00000433389.8; *ESRP2*: NM\_024939.3/ENST00000473183.7; and *CTNND1*:  
156 NM\_001085458.2/ENST00000399050.10.

157 All variants from this study are listed in Table 1 in the supplementary material.

158

### 159 Rare-variants analysis

160 We performed rare variant burden tests using RV-TDT (2) for protein-altering variants in  
161 *ESRP1*, *ESRP2*, and *CTNND1* that had a minor allele frequency less than 0.1% in any  
162 gnomAD population. DenovolyzeR (0.2.0), an R package which compares the observed  
163 number of DNMs to the expected number of DNMs based on a mutational model  
164 developed by Samocha et al. (2014) (63), was used to determine if de novo variants  
165 were enriched in these three genes.

166

### 167 Plasmid generation, site-directed mutagenesis, and mRNA synthesis

168 mRNA from wildtype zebrafish embryos was collected at multiple time points from 6  
169 hours post fertilization (hpf) to 4 days post fertilization (dpf), reverse transcribed, and  
170 combined to make pooled cDNA to clone the *esrp1* coding sequence (CDS). *esrp1* and  
171 *esrp2* were each cloned into a pCS2+8 plasmid backbone using the In-Fusion HD  
172 Cloning Kit (Clontech). The resulting pCS2+8-*esrp2* plasmid was mutagenized with  
173 synonymous mutations surrounding the translational start-site using the GeneArt site-  
174 directed mutagenesis (SDM) system (ThermoFisher) to generate *esrp2* transcripts  
175 resistant to *esrp2* morpholino binding. The 19 human *ESRP1* and *ESRP2* variants were  
176 each individually introduced to the pCS2+8-*esrp1* or MO-resistant pCS2+8-*esrp2*  
177 plasmids through the GeneArt SDM system. All generated pCS2+8 plasmids were  
178 digested with NotI at 37°C for 1hr, and capped mRNA was synthesized using the SP6  
179 mMessage mMachine kit (ThermoFisher).

180 For the murine Py2T transfection experiments, we used the pIBX-C-FF(B)-  
181 mCherry-*esrp1*(2A)-+CKLP plasmid containing the mouse *Esrp1* cDNA sequence, fused  
182 to a mCherry tag (gift from Russ Carstens, University of Pennsylvania). Mouse *Esrp2*  
183 cDNA was purchased from Genomics Online. *Esrp1* cDNA was cloned into the  
184 pcDNA3.1 backbone containing a CMV promoter and SV40 polyA tailing sequence for  
185 expression in mammalian cells using the In-Fusion HD Cloning Kit (Clontech) to  
186 generate the *pcDNA3.1-esrp1-mCherry plasmid*. An mCherry tag was fused in-frame  
187 onto the *Esrp2* cDNA and introduced into the pcDNA3.1 backbone through a multi-insert  
188 in-Fusion cloning strategy, using the pIBX-C-FF(B)-mCherry-*Esrp1*(2A)-+CKLP as the  
189 template for the 2A-mCherry sequence to generate the *pcDNA3.1-esrp2-mCherry*



190 *plasmid*. Selected human *ESRP1* and *ESRP2* gene variants were introduced using the  
191 GeneArt SDM system, as described above.

192

### 193 Zebrafish microinjection and *esrp1/2* rescue assay

194 We previously generated a zebrafish line carrying homozygous loss-of-function alleles  
195 in *esrp1* through CRISPR/Cas9 harboring -4 bp indels which led to a frame shift  
196 mutation and early protein truncation (52). *esrp2* morpholinos (GeneTools) were  
197 reconstituted to a concentration of 8ug/uL in water and stored in single-use aliquots at  
198 RT. 2nL droplets containing (1) 8ng *esrp2* morpholino, (2) 0.05% phenol red and (3)  
199 200pg of *esrp1*, *esrp2*, or *esrp* gene-variant mRNA were microinjected directly into the  
200 cytoplasm of one-cell stage *esrp1*<sup>-/-</sup> zebrafish embryos and grown until 4dpf. (We have  
201 previously shown that the *esrp2* morpholino, injected into *esrp1*<sup>-/-</sup> *esrp2*<sup>wt/wt</sup> is sufficient  
202 to phenocopy the *esrp1*<sup>-/-</sup>; *esrp2*<sup>-/-</sup> phenotype, which is consistent with previous  
203 descriptions (22, 52). Since all the injected embryos were derived from mating of *esrp1*<sup>-/-</sup>  
204 males and females, all animals had the *esrp1*<sup>-/-</sup> genotype and did not require additional  
205 genotyping after phenotype analysis. At 4 dpf, embryos were fixed in 4% formaldehyde,  
206 stained with acid-free Alcian blue as previously described (64), and micro-dissected to  
207 inspect the anterior neurocranium (ANC). The ANC phenotype flatmount was then  
208 scored as wildtype ANC, cleft ANC or rescued ANC.

209

### 210 PY2T cell maintenance and transfection

211 Mouse Py2T cells and *Esrp1/2* DKO Py2T cells were a gift from Russ Carstens from the  
212 University of Pennsylvania (23). Cells were maintained in DMEM supplemented with  
213 10% FBS and penicillin/streptomycin and were not cultured past passage 30. 10.8ug of  
214 plasmid was transfected onto  $10^6$  cells using the 100uL Neon system (ThermoFisher)  
215 with a single, 30 second pulse at 1400V and plated onto 6-well plates. Cells were  
216 harvested for RNA after 24hr, reverse transcribed, and the cDNA was used for RT-PCR  
217 using primers spanning the splice junctions for *Ctnnd1* exons 1 and 3 and *Afhgef11*  
218 exons 36 and 38, Arhgef11 Forward (TCAAGCTCAGAACCAGCAGGAAGT) and  
219 Arhgef11 Reverse (TGCTCGATGGTGTGGAAGATCACA), as described (23). The gels  
220 were quantified by densitometry using Fiji/ImageJ and the results are expressed as  
221 mean  $\pm$  SEM. Statistical analysis involved using GraphPad Prism 9.0 for Windows. The  
222 experiments were performed in triplicate. One-way Anova test, with each comparison  
223 standing alone was used for statistical analysis.  $P < 0.05$  was considered statistically  
224 significant.

225

#### 226 *ctnnd1* mRNA injection into *esrp1*<sup>-/-</sup>; *esrp2*<sup>+/-</sup> intercross

227 To construct the mRNA in vitro transcription (IVT) template, synthetic *Ctnnd1* cDNA,  
228 isoform-201 on Ensembl (ENSDART00000106048.4), was cloned into the linearized  
229 DNA template vector (Takara Bio USA). The plasmid vectors were purified by a  
230 QIAprep spin miniprep kit (QIAGEN). The plasmid was digested with Hind III HF (NEB  
231 Biolabs) at 37°C for 1hr, 80°C for 20 minutes for inactivation and mRNA was  
232 synthesized using the T7 MEGAscript kit (ThermoFisher).

233 For micro-injection, progeny of *esrp1*<sup>-/-</sup>; *esrp2*<sup>+/-</sup> inter-cross, previous described  
234 by Carroll, 2020 (52) were injected at the single cell stage with either 250 pg of *ctnnd1*  
235 mRNA (along with water), or *gfp* mRNA, for controls. Injected embryos were raised to 4  
236 dpf, at which time embryos were fixed in 4% formaldehyde, stained with acid-free Alcian  
237 blue, and microdissected to inspect the anterior neurocranium (ANC). The ANC was  
238 scored as wildtype ANC or cleft ANC. Additionally, the pectoral fins were also analyzed  
239 and scored as wildtype fin or curled fin. For the otolith phenotype, wildtype was scored  
240 when the otoliths were separate and the mutant phenotype when the otoliths were  
241 fused. For the paired bilateral structures, if one fin was curled or one set of otoliths were  
242 fused, the animal was scored as mutant. After the phenotypic assessments for ANC, fin  
243 and otoliths, both the mRNA injected embryos and the control injected embryos was  
244 tracked and individually genotyped. Whenever there is an animal with genotype of  
245 *esrp1*<sup>-/-</sup>; *esrp2*<sup>-/-</sup> but exhibited ANC that are not fully cleft, fins that are not fully curled  
246 and separate otoliths, these animals were scored as rescues.

247

#### 248 RNA in situ hybridization staining (RNAScope and BaseScope)

249 Wildtype and *esrp1*<sup>-/-</sup>; *esrp2*<sup>+/-</sup> zebrafish were crossed and the progeny embryos raised  
250 to 4 dpf. The *esrp1*<sup>-/-</sup>; *esrp2*<sup>-/-</sup> double mutant embryos were scored at 4 dpf based on the  
251 abrogated pectoral fin phenotype. The wild type and *esrp1*<sup>-/-</sup>; *esrp2*<sup>-/-</sup> embryos were  
252 fixed in 4% formaldehyde, taken through a sucrose gradient, and then cryo embedded  
253 and sectioned. RNAScope probes were designed with assistance from ACDBio to target  
254 the region of 700-1661 base pairs of the RNA for DR Ctnnd1 XM\_021476936.1, which  
255 corresponds to ENSDART00000106048.4 for ensemble 201.

256            Additionally, RNAScope and BaseScope probes were designed for murine *Esrp1*  
257 (we have previously shown that *Esrp1* and *Esrp2* colocalize in the oral epithelium) (52).  
258 Hybridization and staining were performed according to the manufacturers protocol.  
259 Stained sections were imaged on a Leica SP8 confocal microscope where a Z-stack  
260 was obtained and analyzed on imageJ software to obtain optimal images. BaseScope  
261 probes were designed and purchased from ACDBio to specifically target the *Ctnd1*  
262 long and short isoforms. Staining was carried out according to the manufacturer's  
263 protocols on both fixed, frozen, and sectioned wildtype and *Esrp1/2* DKO at E15.  
264 Stained sections were imaged as above.

265

#### 266 Statistics and Reproducibility

267 The results are expressed as percentage or as mean  $\pm$  SEM. Statistical analysis was  
268 using GraphPad Prism 10 for Windows (GraphPad Software, San Diego,  
269 CA, [www.graphpad.com](http://www.graphpad.com)). All experiments were performed at least in triplicate. Two-way  
270 analysis of variance or Student *t* test was used for statistical analysis.  $P < 0.05$  was  
271 considered statistically significant.

272

## 273 Results

### 274 ***esrp1* and *esrp2* are required for morphogenesis of epithelial derived tissues**

275 We previously described the genetic requirement of *esrp1/2* in zebrafish epithelial  
276 development, disruption of which resulted in tethering of the upper mouth opening  
277 extending into a separation of the anterior neurocranium, a phenotype morphologically  
278 analogous to CL/P of amniotes (52). Given the expression of *esrp1/2* and in periderm  
279 and embryonic epithelial cells broadly, we examined other structures formed by  
280 epithelial origins. It was reported that *Esrp1* regulated the alternative splicing of  
281 *Arhgef11*, which was described to be important for proper otoliths development in  
282 zebrafish (65). When the *esrp1/2* double mutants were examined at 4 dpf, we  
283 discovered that more than 90% of the mutant larvae exhibited at least one fused otolith  
284 (Figure 1A, B).

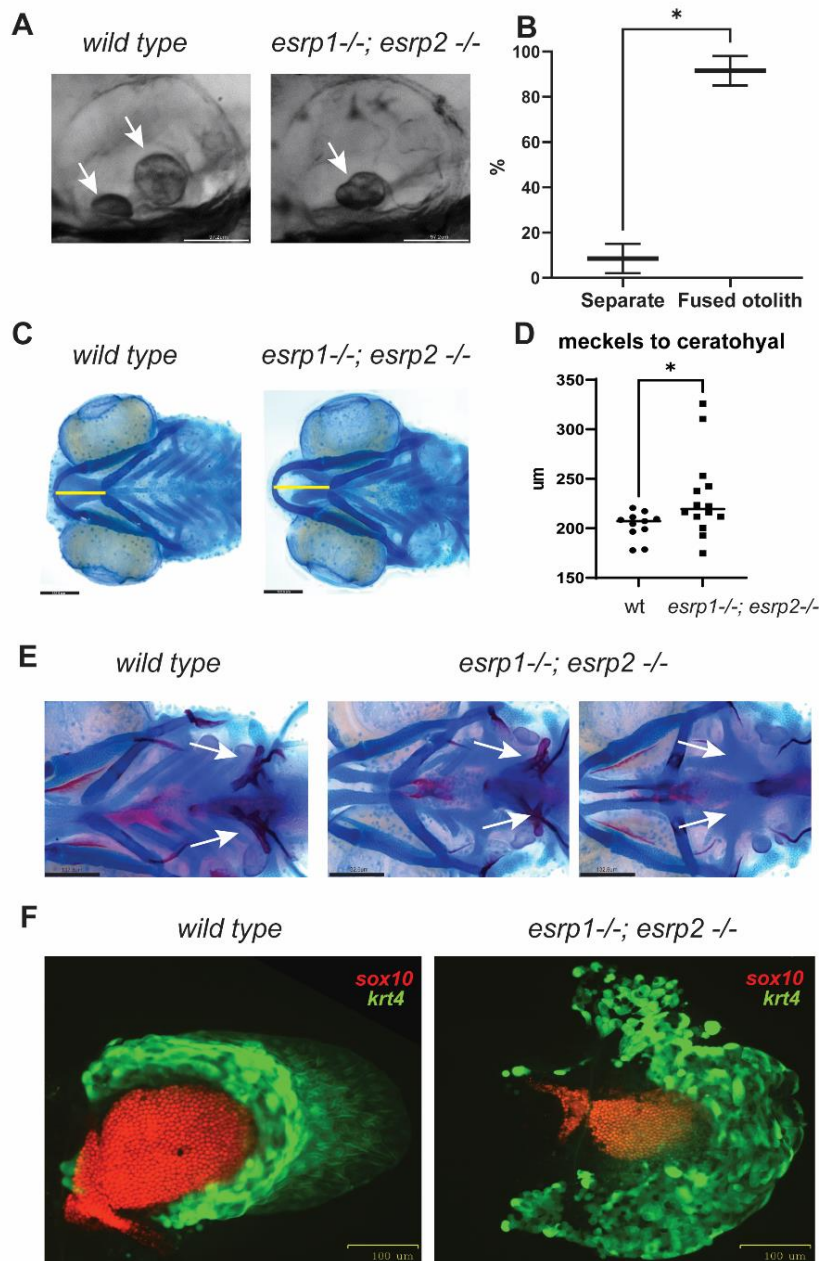
285 Ventral cartilages that form with epithelial-mesenchymal interactions were also  
286 dysmorphic, where the Meckel's cartilage appeared longer in the antero-posterior axis  
287 and narrower in the coronal axis. These morphologic differences can be captured by  
288 measuring the distance between Meckel's and ceratohyal cartilages which is extended  
289 in the *esrp1/2* mutants (Figure 1C, D). We also detected partial penetrance of loss of  
290 ceratobranchial cartilages in 30% of the *esrp1/2* double mutant larvae at 7 dpf, and  
291 these larvae also exhibited loss of pharyngeal teeth (Figure 1E).

292 Epithelial-mesenchymal interaction is also required for pectoral fin development.  
293 We observed that the *esrp1/2* double mutants exhibit foreshortened and curled pectoral  
294 fins, where the *sox10* labeled chondrocytes that populate the mesenchymal component

295 and the *krt4* labeled epithelial populations are both decreased in cell number in the  
296 *esrp1*<sup>-/-</sup>; *esrp2*<sup>-/-</sup> fins at 4 dpf (Figure 1F). Whereas the wildtype fins extend and fan out  
297 as they develop to 4 dpf, the fins in the *esrp1*<sup>-/-</sup>; *esrp2*<sup>-/-</sup> larvae curl proximally and are  
298 typically stuck to the torso through epithelial attachments (Figure 6A).

299

**Figure 1**



300 **Figure 1. *esrp1* and *esrp2* are required for morphogenesis of epithelial derived tissue:**  
 301 **otoliths, pharyngeal teeth and pectoral fins. (A)** zebrafish otoliths indicated by white arrows  
 302 at 72 hpf. **(B)** Quantification and t test of zebrafish otoliths from genotyped mutants  
 303 characterized as separate or fused otoliths. t-test, n=75. **(C)** Alcian blue representation of a 6  
 304 dpf zebrafish wildtype and *esrp1<sup>-/-</sup> esrp2<sup>-/-</sup>* double mutant showing cartilage stain, yellow line  
 305 shows the measurement of the distance between the midline of Meckel's and ceratohyal  
 306 cartilages. **(D)** quantification and t-test analysis of this measurement in wildtype (n=11) and  
 307 *esrp1<sup>-/-</sup>; esrp2<sup>-/-</sup>* mutants (n=14). **(E)** Alcian blue and Alizarin red staining of larvae at 7 dpf  
 308 ventral view, the pharyngeal teeth are present in wildtype (white arrows). In contrast, the *esrp1<sup>-/-</sup>*  
 309 *; esrp2<sup>-/-</sup>* all exhibit decreased number of teeth, and occasionally some double mutants lack all  
 310 ceratobranchial cartilages and the pharyngeal teeth are absent. **(F)** wildtype and *esrp1<sup>-/-</sup> esrp2<sup>-/-</sup>*  
 311 mutant pectoral fins labeled with *sox10* mCherry (red) and *krt4* gfp (green).

312 ***In vitro* and *in vivo* assays to functionally test *ESRP1* and *ESRP2* human gene**  
313 **variants.**

314 In a previous study we showed that *esrp1*<sup>-/-</sup>; *esrp2*<sup>+/-</sup> intercross yielded Mendelian ratio  
315 of 25% *esrp1*<sup>-/-</sup>; *esrp2*<sup>-/-</sup>, and that injection of morpholino against *esrp2* in the *esrp1*<sup>-/-</sup>  
316 mutant embryos can consistently phenocopy the *esrp1*<sup>-/-</sup>; *esrp2*<sup>-/-</sup> double mutant  
317 (Figure 2A) (52). This *esrp1*<sup>-/-</sup>; *esrp2* MO model provides significant advantages over  
318 *esrp1*<sup>+/-</sup>; *esrp2*<sup>+/-</sup> intercross, as the entire clutch of the *esrp1*<sup>-/-</sup> embryos injected with  
319 *esrp2* MO consistently exhibited the cleft ANC phenotype greatly facilitating detection of  
320 rescue of injected *ESRP1/2* mRNA to be tested.

321 We found that over-expression of wildtype zebrafish and human *ESRP1* and  
322 *ESRP2* mRNA rescued the cleft ANC phenotype in *esrp1*<sup>-/-</sup>; *esrp2* MO embryos (Figure  
323 2B) (52). Alcian blue staining of *esrp1*<sup>-/-</sup>; *esrp2*<sup>-/-</sup> zebrafish at 4 dpf revealed a cleft ANC  
324 phenotype where a population of chondrocytes in the medial ANC is absent. A similar  
325 phenotype is observed when translation-blocking anti-*esrp2* morpholinos were injected  
326 into *esrp1*<sup>-/-</sup> embryos (Figure 2A).

327 To functionally test human *ESRP1* or *ESRP2* gene variants, we introduced point  
328 mutations into zebrafish *esrp1* or *esrp2* coding sequences and subsequently co-inject  
329 8ng of anti-*esrp2* MO with either: (1) capped *esrp1* mRNA, (2) capped *esrp2* mRNA  
330 mutagenized with synonymous mutations at the MO binding site, or (3) either *esrp1*  
331 mRNA encoding for human *ESRP1* gene variants of unknown significance, or (MO-  
332 resistant) *esrp2* mRNA encoding for human *ESRP2* gene variants of unknown  
333 significance. We hypothesized that benign variants that preserve protein function would  
334 robustly rescue the cleft ANC phenotype like native *esrp1* or *esrp2* mRNA. Conversely,

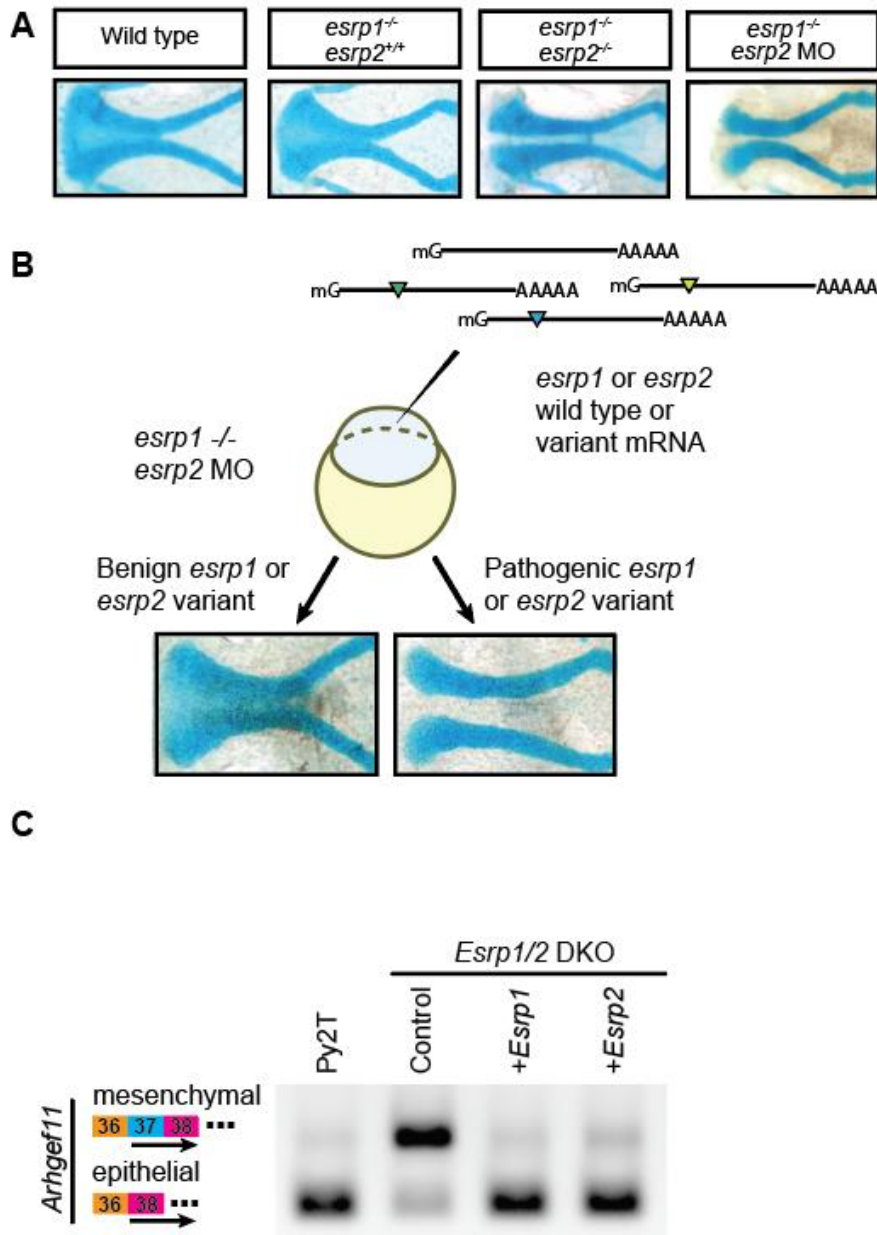


335 pathogenic human *ESRP1/2* gene variants with loss-of-function would fail to rescue the  
336 cleft ANC phenotype (Figure 2B). Human *ESRP1* and *ESPR2* gene variants were  
337 cloned by site directed mutagenesis, and synthesized mRNA was injected with *esrp2*  
338 MO into one-cell stage *esrp1*<sup>-/-</sup> embryos. The *esrp2* cDNA was engineered to prevent  
339 hybridization of the *esrp2* MO to the synthesized mRNA.

340 In order to gain additional functional assessment of the gene variants, we  
341 developed an independent *in vitro* assay using *Esrp1/2* mutant Py2T cells (66). The  
342 murine Py2T epithelial cell line was developed where *Esrp1* and *Esrp2* were ablated  
343 using CRISPR-mediated gene editing. The *Esrp1/2*<sup>-/-</sup> Py2T cells exhibited splicing  
344 deficiencies in the *Esrp* target gene, *Arhgef11* (Figure 2C) (66). RT-PCR performed on  
345 wildtype Py2T cell cDNA using primers spanning splice junctions for *Arhgef11*  
346 demonstrated the presence of two major isoforms. The difference between these two  
347 isoforms is the presence or absence of exon 37, which is included in mesenchymal  
348 cells, but skipped in Py2T epithelial cells (23, 67, 68). Py2T cells carrying *Esrp1* and  
349 *Esrp2* loss-of-function alleles preferentially expressed the longer mesenchymal isoform  
350 of *Arhgef11*.

351 We found that over-expression of *Esrp1* or *Esrp2* in the *Esrp1/2* DKO Py2T cells  
352 efficiently rescued RNA-splicing to generate the epithelial isoform of *Arhgef11* transcript  
353 (Figure 2C).

**Figure 2**



354 **Figure 2. Complementary *in vivo* and *in vitro* functional assays to test human *ESRP1* and**  
 355 ***ESRP2* gene variants. (A)** Microdissected ANC of Alcian-blue stained embryos at 4 dpf for  
 356 wild-type, *esrp1*<sup>-/-</sup>; *esrp2*<sup>+/+</sup>, *esrp1*<sup>-/-</sup>; *esrp2*<sup>-/-</sup>, and *esrp1*<sup>-/-</sup>; *esrp2* MO embryos. **(B)** Schematic for  
 357 the *esrp* morphant variant assay in zebrafish. Variants that robustly rescued the cleft ANC  
 358 phenotype were scored as benign, while variants that failed to rescue the cleft ANC phenotype  
 359 were scored as pathogenic. **(C)** RT-PCR was performed using primers spanning exons 36-38 of  
 360 *Arhgef11* on cDNA isolated from wild-type mouse Py2T cells, *Esrp1/2* double-knockout Py2T  
 361 cells, or *Esrp1/2* double-knockout Py2T cells electroporated with plasmids encoding for either  
 362 *Esrp1* or *Esrp2* genes. Arrow markers point to the epithelial (short) isoform and mesenchymal  
 363 (long) isoform retaining exon 37.

## 364 **Identifying human *ESRP1* and *ESRP2* gene variants**

365 Genome sequencing efforts have deposited numerous gene variants in publicly  
366 available repositories, including the Gabriella Miller Kids First (GMKF) Pediatric  
367 Research Program and ClinVar (69-71). We filtered sequencing data from the both  
368 repositories for patients with OFC or autosomal recessive deafness (20, 58) and  
369 identified gene variants for either *ESRP1* or *ESRP2* to generate a list of 32 potentially  
370 disease-associated gene variants.

371         Because we are utilizing *in vivo* assay in zebrafish and *in vitro* assay in murine  
372 Py2T cells, we prioritized those human *ESRP1* and *ESRP2* gene variants residing in  
373 cross-vertebrate conserved residues. For *ESRP1*, the overall amino acid sequence  
374 identity was 97% and 64.68% between humans and mice, or humans and zebrafish,  
375 respectively. However, when focusing on the RNA-recognition motif (RRM) domains of  
376 *ESRP1*, the similarity of the sequences between humans and mice and humans and  
377 zebrafish increased to 98.82% and 94.12% for RRM1, 99.08% and 79.82% for RRM2,  
378 and 95.06% and 77.78% for RRM3. Similarly, for *ESRP2*, the overall amino acid  
379 sequence similarity was 98.67% between humans and mice and 85.33% between  
380 humans and zebrafish. The domain-specific amino acid sequence similarities were  
381 98.67% and 85.33% for RRM1, 98.13% and 81.31% for RRM2, and 96.3% and 77.78%  
382 for RRM3 between humans and mice, and humans and zebrafish, respectively.  
383 Altogether, we identified 19 out of the 32 gene variants in residues fully conserved  
384 between human, mouse, and zebrafish. Gene variants were evenly spread throughout  
385 both proteins and included two variants in the RRM1 domain of *ESRP1* and two variants

386 each in the RRM1, RRM2, and RRM3 domains of *ESRP2* (Figure 1 Supplementary  
387 Material).

388 We found that the *in silico* predictions from SIFT and Polyphen-2 followed one of  
389 four patterns: (1) concordant predictions from both tools annotating the variant as  
390 benign, (2) concordant predictions from both tools annotating the variant as damaging,  
391 (3) discordant predictions from both tools, (4) tools unable to predict the effect of the  
392 variant on protein function (Table 1). Altogether, two variants from *ESRP1* (E194A and  
393 N643S) and two variants from *ESRP2* (C372S and T475T) were predicted by both SIFT  
394 and PolyPhen-2 to have a benign effect on protein function. One variant from *ESRP1*  
395 (Q90R) and four from *ESRP2* (R250Q, R315H, R353Q, and R667C) were predicted by  
396 both to have a deleterious effect on protein function. SIFT and PolyPhen-2 do not offer  
397 predictions for three truncation variants (*ESRP1* D222fs, *ESRP2* R520\*, and *ESRP2*  
398 E547del). However, the remaining three *ESRP1* variants (L259V, K287R and Y605F)  
399 and four *ESRP2* variants (L92Q, S508L, R437H, and L665W) had discordant  
400 predictions between both algorithms. Thus, *in silico* predictions were not adequate to  
401 annotate roughly half of the selected gene variants and required an alternate approach  
402 to predict their effects on protein function.

403

404

405

406

407

408

409

410

411 **Table 1: *ESRP1* and *ESRP2* variants classification**

ESRP1	Protein Domain	PolyPhen-2	SIFT	Alpha Missense	Zf in vivo assay	Py2T in vitro assay	Interpretation
Q90R		Damaging	Damaging, LC	Benign	Rescue	n/a	Benign
E194A		Benign	Benign	Benign	Rescue	n/a	Benign
D222fs		n/a	n/a	n/a	Mutant	Deficient	Damaging
L259V	RRM1	Damaging	Benign	Pathogenic	Rescue	Restored	Benign
K287R	RRM1	Damaging	Benign	Benign	Rescue	n/a	Benign
Y605F		Benign	Damaging, LC	Benign	Rescue	n/a	Benign
N643S		Benign	Benign	Benign	Rescue	Restored	Benign

412

ESRP2	Protein Domain	PolyPhen-2	SIFT	Alpha Missense	Zf in vivo assay	Py2T in vitro assay	Interpretation
L92Q		Benign	Damaging, LC	Likely pathogenic	Rescue	n/a	Benign
R250Q		Damaging	Damaging	Likely pathogenic	Rescue	Restored	Benign
R315H	RRM1	Damaging	Damaging	Likely pathogenic	Mutant	Deficient	Damaging
R353Q	RRM1	Damaging	Damaging	Likely pathogenic	Rescue	Restored	Benign
C372S	RRM2	Benign	Benign	Ambiguous	Rescue	n/a	Benign
R437H	RRM2	Damaging	Benign	Ambiguous	Rescue	n/a	Benign
T475T	RRM3	Benign	Benign	n/a	Rescue	Restored	Benign
S508L	RRM3	Damaging	Benign	Likely pathogenic	Rescue	Restored	Benign
R520STOP	RRM3	n/a	n/a	n/a	Mutant	Deficient	Damaging
E547del	RRM3	n/a	n/a	n/a	Rescue	n/a	Benign
L665W		Benign	Damaging, LC	Likely benign	Rescue	n/a	Benign
R667C		Damaging	Damaging, LC	Ambiguous	Rescue	Restored	Benign

413

414 **Functional testing of *ESRP1* and *ESRP2* variants in zebrafish and murine Py2T**  
 415 **cell assays**

416 The selected 19 *ESRP1* and *ESRP2* gene variants were experimentally tested in  
 417 zebrafish and Py2T cell assays. Site-directed mutagenesis was carried out in *ESRP1*  
 418 and *ESRP2* cDNA sequences and cloned into the pCS2+8 vector backbone to generate  
 419 capped mRNA for microinjection into zebrafish embryos. The zebrafish assay was  
 420 optimized by microinjection of *esrp2* translation-blocking morpholinos into *esrp1*<sup>-/-</sup>  
 421 intercross, because the *esrp2*<sup>-/-</sup> females are infertile (22). However, since the *esrp2* MO  
 422 would also neutralize exogenous injected *ESRP2* mRNA upon co-injection into

423 zebrafish embryos, synonymous mutations were introduced in the translational start site  
424 of the pCS2+8-*Esrp2* plasmid, to generate *esrp2* MO-resistant *ESRP2* mRNA  
425 transcripts. Co-injection of 8ng of *esrp2* MO with 200pg of either *ESRP1* mRNA or MO-  
426 resistant *ESRP2* mRNA fully rescued the ANC phenotype in over 75% of 19 injected  
427 clutches at 4 dpf (Figure 3A).

428 To test for the ability of human *ESRP1/2* gene variants to rescue the cleft ANC  
429 phenotype in zebrafish, each of the 19 *ESRP1* or *ESRP2* gene variants was co-injected  
430 with *esrp2*-MO into *esrp1*<sup>-/-</sup> zebrafish embryos. At 4 dpf, the injected fish were fixed,  
431 stained with Alcian Blue, and analyzed. We found that for *ESRP1*, all 6 missense  
432 variants rescued the ANC phenotype. Only one variant, a frameshift mutation at the 222  
433 aspartate residue (D222fs), had a large proportion of cleft ANC in the injected clutch  
434 compared to embryos injected with wildtype *esrp1* mRNA, and was scored as a  
435 pathogenic variant (Figure 3B). For *ESRP2*, 10 out of 12 tested gene variants rescued  
436 the ANC phenotype, in a ratio like the *esrp2* mRNA control and were scored as benign  
437 variants. The silent mutation T475T, served as an internal negative control and also  
438 scored as benign. The remaining 2 *ESRP2* gene variants (R315H and R520\*) failed to  
439 rescue the ANC phenotype and were scored as pathogenic (Figure 3C).

440 To independently assess the gene variant functional testing results obtained from  
441 the zebrafish model, we tested 3 *ESRP1* and 8 *ESRP2* human gene variants using the  
442 mouse Py2T cell assay, with epithelial-specific RNA splicing of *Arhget11* as the readout  
443 (Figure 3D, 3E). We aimed to obtain an additional functional assessment for those gene  
444 variants testing results that contradicted *in silico* prediction. We performed site-directed  
445 mutagenesis to introduce the 11 gene variants, that were electroporated into *Esrp1/2*

446 DKO PY2T cells and performed the RT-PCR assay 24 hours post-electroporation. We  
447 found that for *ESRP1*, gene variant L259V restored *Arhgef11* restriction to the epithelial  
448 isoform was scored as damaging for Polyphen-2 and Alpha missense and benign for  
449 SIFT (Figure 3, Table 1). The frameshift variant, D222fs, that was pathogenic in the in  
450 vivo assay was also pathogenic in this assay as it was unable to restore the epithelial  
451 isoform (Figure 3D, Table 1). Interestingly, the *ESRP1* gene variant N643S partially  
452 restored some of the splicing function of *Esrp1*, where both epithelial and mesenchymal  
453 *Arhgef11* isoforms were detected in a 1:1 ratio (Figure 3D). However, the same variant,  
454 N643S, in zebrafish rescued the phenotype. Statistical analysis for the Py2T rescue  
455 assay, can be found at Supplementary Figure 2. These results suggest that *ESRP1*  
456 N643S variant may be hypomorphic, or that *Arhgef11* is just one readout of *Esrp1*  
457 mRNA splicing activity. Because *Esrp1* shows position-dependent repression of exon  
458 splicing of *Arhgef11*, it is possible that some domains or regions may be required, or  
459 not, for some specific functions. It is possible that some splicing events may be  
460 differentially affected by mutations and there are other suggested functions of *Esrp1* in  
461 mRNA stabilization or post-transcriptional regulation that are accounted for in the  
462 zebrafish rescue assay (60).

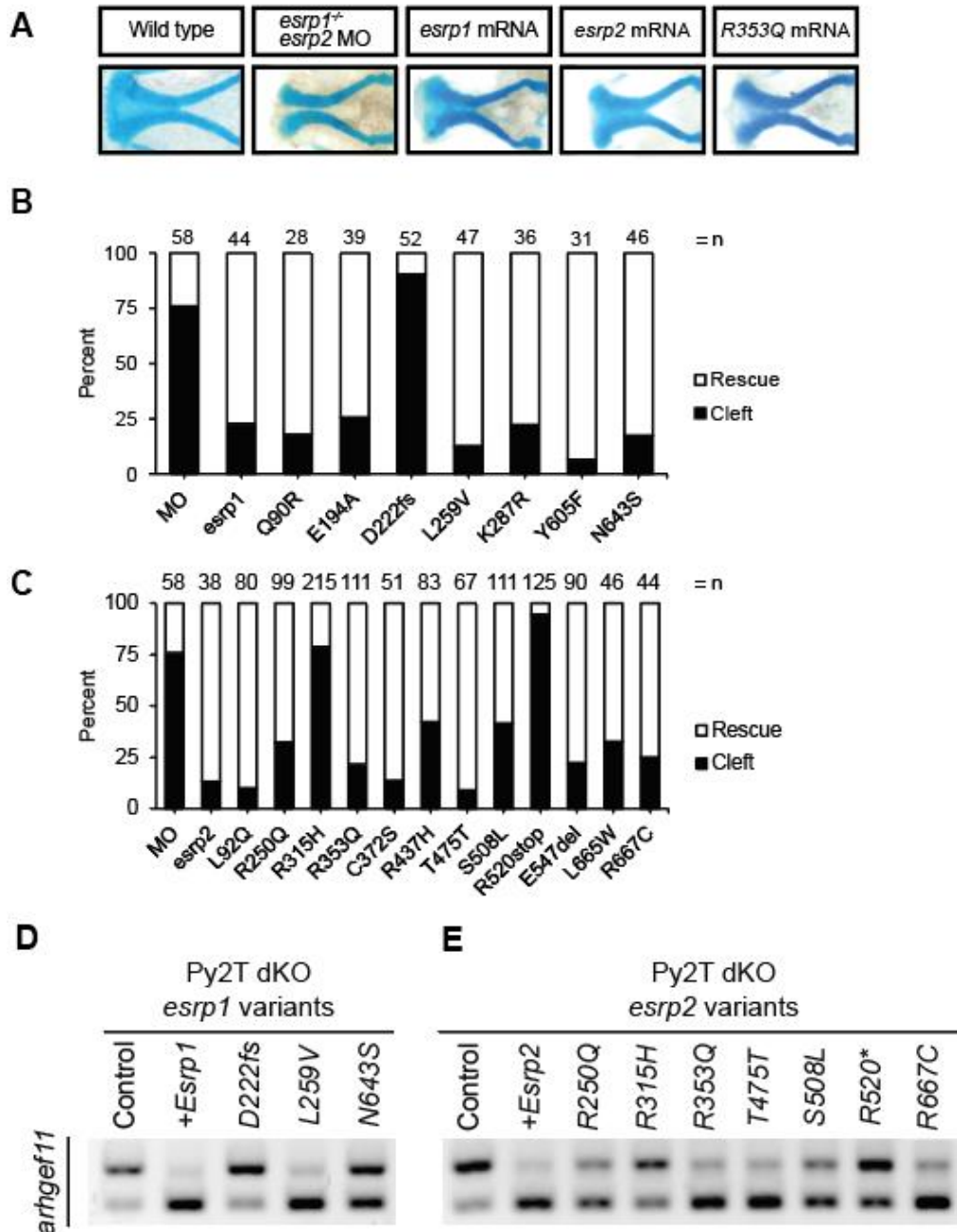
463 For *ESRP2*, variants R250Q, R353Q and R667C rescued the molecular splicing  
464 of *Arhgef11* in the Py2T assay, (Figure 3E, Table 1). However, *ESRP2* gene variants  
465 R315H, S508L, and R520\* failed to rescue deficient *Arhgef11* splicing in the Py2T  
466 assay and were scored as pathogenic, corroborating the pathogenic scoring from the  
467 zebrafish ANC rescue assay (Figure 3E, Table 1).

468 Overall, we found that the *in vivo* zebrafish ANC rescue assay and the *in vitro*  
469 Py2T splicing assays were largely concordant to determine pathogenicity of the *ESRP1*  
470 and *ESRP2* gene variants tested. PolyPhen-2 correctly predicted the effect of 8/18  
471 (44.4%) tested gene variants, while SIFT correctly predicted the effect of 7/18 (38.8%)  
472 gene variants. When the predictions of both algorithms were concordant, they correctly  
473 predicted the consequence of 5 out of 7 (71.4%) gene variants on protein function  
474 (Table 1). The performance of concordant predictions was better for annotating benign  
475 variants where the algorithms correctly identified all four concordant benign variants  
476 with benign effects in both of our assays. Strikingly, the computational agreement  
477 incorrectly annotated 2 of 4 (50%) gene variants as pathogenic that had benign effects  
478 in both rescue assays. Ultimately, the algorithmic predictions were unable to determine  
479 half of the identified gene variants and greatly overestimated the prevalence of  
480 pathogenic variants (Table 1).

481



### Figure 3



482 **Figure 3. Functional testing of human ESRP1 and ESRP2 gene variants. (A)**  
 483 Representative images of the ANC from Alcian-blue stained larvae at 4 dpf after injection with  
 484 *esrp2* MO and 200pg of: *esrp1* mRNA, *esrp2* R353Q mRNA. ANC was scored as a rescued  
 485 ANC or cleft ANC **(B)** *ESRP1* and **(C)** *ESRP2* gene variant rescue assay results for embryos  
 486 injected with *esrp2* MO and 200pg of *esrp1* variant mRNA. Results presented as percentage of  
 487 rescue vs. cleft as different numbers of embryos survived and were analyzed, indicated as n  
 488 above each bar. **(D)** *ESRP1* and **(E)** *ESRP2* gene variant rescue assay by detecting alternative  
 489 splicing of Arhgef11 in murine Py2T wildtype and *Esrp1*<sup>-/-</sup>; *Esrp2*<sup>-/-</sup> double knockout cells.  
 490

## 491 **AlphaMissense over-interpreted pathogenic variants**

492           Recently a new gene variant analysis tool AlphaMissense was released and  
493 purported to improve variant calling accuracy by leveraging protein structure information  
494 predicted by machine learning algorithm AlphaFold (72). Using AlphaMissense to  
495 analyze the 6 *ESRP1* and 9 *ESRP2* missense variants we had functionally tested, we  
496 observed that AlphaMissense classified 5 variants as benign for *ESRP1* (Q90R, E194A,  
497 K287R, Y605F, N643S) consistent with the functional tests, but called L259V as  
498 pathogenic when both the *in vivo* and *in vitro* functional tests demonstrated protein  
499 function (Figure 4).

500           For *ESRP2*, AlphaMissense and the experimental validation were only  
501 concordant on 2 variants out of 9, calling R315H as pathogenic and L665W as benign  
502 (Figure 4). AlphaMissense called 6 variants as pathogenic when they were shown to be  
503 functionally benign in both *in vitro* and *in vivo* functional tests. Therefore, our results  
504 showed that AlphaMissense may over-interpret variants as pathogenic for some genes.

505

506

507

508

509

510

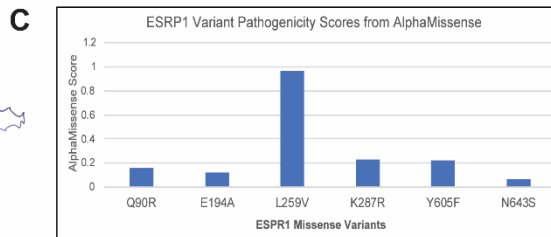
511

## Figure 4

### ESRP1

**A**

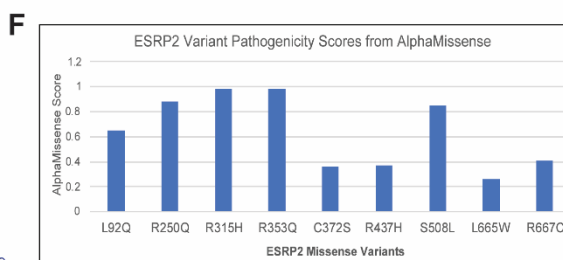
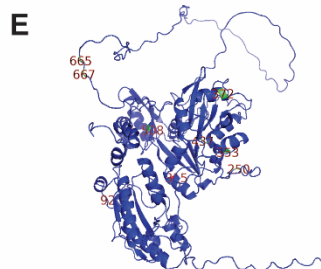
ESRP1	Variants	AlphaMissense Mutation Score	AlphaMissense Category	Functional Results
Q6NXG1	Q90R	0.1558	Benign	Benign
Q6NXG1	E194A	0.1192	Benign	Benign
Q6NXG1	L259V	0.9676	Pathogenic	Benign
Q6NXG1	K287R	0.2256	Benign	Benign
Q6NXG1	Y605F	0.2212	Benign	Benign
Q6NXG1	N643S	0.0665	Benign	Benign



### ESRP2

**D**

ESRP2	Variants	AlphaMissense Mutation Score	AlphaMissense Category	Functional Results
ENST00000473183.7	L92Q	0.6475	Likely Pathogenic	Benign
ENST00000473183.7	R250Q	0.8854	Likely Pathogenic	Benign
ENST00000473183.7	R315H	0.9855	Likely Pathogenic	Damaging
ENST00000473183.7	R353Q	0.9827	Likely Pathogenic	Benign
ENST00000473183.7	C372S	0.3612	Ambiguous	Benign
ENST00000473183.7	R437H	0.3702	Ambiguous	Benign
ENST00000473183.7	S508L	0.8522	Likely Pathogenic	Benign
ENST00000473183.7	L665W	0.2644	Likely Benign	Benign
ENST00000473183.7	R667C	0.4095	Ambiguous	Benign



512

513 **Figure 4. AlphaMissense pathogenicity predictions for ESRP1 and ESRP2 missense**  
 514 **variants.** *ESRP1* and *ESRP2* gene variants from OFC cases in the GMFK Children's dataset  
 515 and ClinVar variants associated with cleft lip and/or palate or autosomal recessive deafness  
 516 were identified. 6 *ESRP1* and 9 *ESRP2* (A and D) missense variants were analyzed using the  
 517 AlphaMissense (AM) model. The tables (C and F) show the AM-predicted pathogenicity  
 518 compared to our functional test results and the AM mutation score, which is also graphed. On  
 519 the left, the *ESRP1* and *ESRP2* AlphaFold structures (B and E), with labeled missense  
 520 mutations, color-coded with the functional results.

521 **Alternative splicing to generate epithelial isoform of *Ctnnd1* requires *Esrp1/2***  
522 **function**

523 We and others demonstrated that *Esrp1* and *Esrp2* regulate the alternative splicing of  
524 *Ctnnd1*, generating isoforms that differ between epithelial and mesenchymal cell types  
525 (20, 60, 66, 73), making *Ctnnd1* an interesting *Esrp1/2* target that has also been  
526 implicated in CL/P (61).

527 *CTNND1* (p120-catenin) have been associated with Blepharochelidontic (BCD)  
528 syndrome and non-syndromic human CL/P (19, 20, 74). Like other catenins, *Ctnnd1* has  
529 dual roles: it functions as part of the adherens junction cellular scaffolding to stabilize  
530 cell adhesion molecules, as well as a transcriptional regulator (19, 75-79). Furthermore,  
531 functional differences between epithelial and mesenchymal forms of *Ctnnd1* have been  
532 described (80-82). Four major isoforms for *Ctnnd1* have been characterized in humans.  
533 The full-length isoform, isoform 1, has a translational start site at the first methionine in  
534 the sequence (1 Met), while isoforms 2, 3, and 4 undergo splicing events that cause a 5'  
535 truncation of the transcript and change the translational start site to methionines 55,  
536 102, and 324, respectively. Isoform 1 of *CTNND1* is predominantly expressed in the  
537 mesenchyme, while the shorter isoform 3 is restricted to the epithelium. The remaining  
538 isoforms, 2 and 4, are less abundant and have not been thoroughly characterized (74).

539 When we aligned the amino acid sequences between human, mouse, and  
540 zebrafish *Ctnnd1* homologs, we found that methionine in positions 1 and 102 are  
541 conserved in all three species. Methionine 55 is part of a 14 aa stretch absent in  
542 zebrafish (Figure 5A). Given that transcripts for the long (mesenchymal) isoform shifts  
543 to the shorter (epithelial) isoform by splicing out a 5' exon(s) and moving down to a

544 conserved methionine, splicing patters are well-conserved across human, mouse, and  
545 zebrafish. Cox et. al reported that *ESRP2* and a short form of the full-length *CTNND1*  
546 protein, identified by an antibody to the C-terminus, are colocalized in the periderm of  
547 human embryos (20). Meanwhile, RNA splicing of *Ctnnd1* transcripts is deficient in the  
548 embryonic epithelium of *Esrp1*<sup>-/-</sup> mice (53).

549 We confirmed that long and shorter *Ctnnd1* isoforms were found in the mouse  
550 Py2T cells by performing RT-PCR using primers spanning exon 2, which is partially  
551 skipped in the shorter isoform for *Ctnnd1*. In the *Esrp1/2*<sup>-/-</sup> Py2T cell line, the splicing  
552 pattern of *Ctnnd1* shifts and is biased towards the longer mesenchymal isoform,  
553 confirming previous observations (60).

554 To localize *Ctnnd1* and *Esrp1/2* gene expression in wildtype mouse and  
555 zebrafish, we carried out RNAscope and BaseScope on wildtype and mutant mouse  
556 and zebrafish sections (Figure 5B 5C). The *Ctnnd1* probe used identifies shared C-  
557 terminal exons shared in all *Ctnnd1* isoforms. Only *Esrp1* probe was used here as we  
558 and others have previously shown that *Esrp1* and *Esrp2* gene expression are co-  
559 localized in mouse and zebrafish (21, 22, 52, 66). In zebrafish, *ctnnd1* and *esrp1*  
560 RNAscope signals are co-localized robustly throughout the oral epithelium with sparse  
561 signals in the mesenchyme.

562 To assess the tissue specific distribution of the longer mesenchymal isoforms of  
563 *Ctnnd1* vs. shorter epithelial isoform, BaseScope probes were used to detect the two  
564 *Ctnnd1* isoforms from wildtype and *Esrp1*<sup>-/-</sup>; *Esrp2*<sup>-/-</sup> mutant mouse at E15. Similar to  
565 RNAscope result in zebrafish (Figure 5B), the murine *Ctnnd1* BaseScope signals for  
566 both mesenchymal and epithelial isoforms were robust in the oral epithelium and

567 sparsely scattered in the mesenchyme (Figure 5D and 5G). When signal is  
568 differentiated by isoform, the longer *Ctnnd1* mesenchymal isoform was uniformly  
569 distributed throughout the epithelium and mesenchyme (5E and 5H). However, the  
570 shorter *Ctnnd1* epithelial isoform was restricted to the epithelial cells and excluded from  
571 the muscle (5F and 5I). In the wildtype, BaseScope signals of the longer *Ctnnd1*  
572 mesenchymal isoform appeared equally distributed in the mesenchyme and epithelium,  
573 and the signals of the shorter isoform was epithelial restricted. In the *Esrp1*<sup>-/-</sup>; *Esrp2*<sup>-/-</sup>  
574 mutant mouse, *Ctnnd1* transcript level was significantly reduced and predominantly the  
575 longer *Ctnnd1* mesenchymal isoform was detected, in both the mesenchyme and  
576 epithelium. The shorter *Ctnnd1* epithelial isoform was sparsely detected via BaseScope  
577 in the *Esrp1*<sup>-/-</sup>; *Esrp2*<sup>-/-</sup> mutant, consistent with the finding where shorter isoform was  
578 significantly reduced in the *Esrp1*<sup>-/-</sup>; *Esrp2*<sup>-/-</sup> Py2T cells by qPCR. These results  
579 corroborate that *Esrp1/2* is required for RNA splicing of *Ctnnd1*, generating the shorter  
580 isoform specifically in the epithelium but not the mesenchyme.

581

582

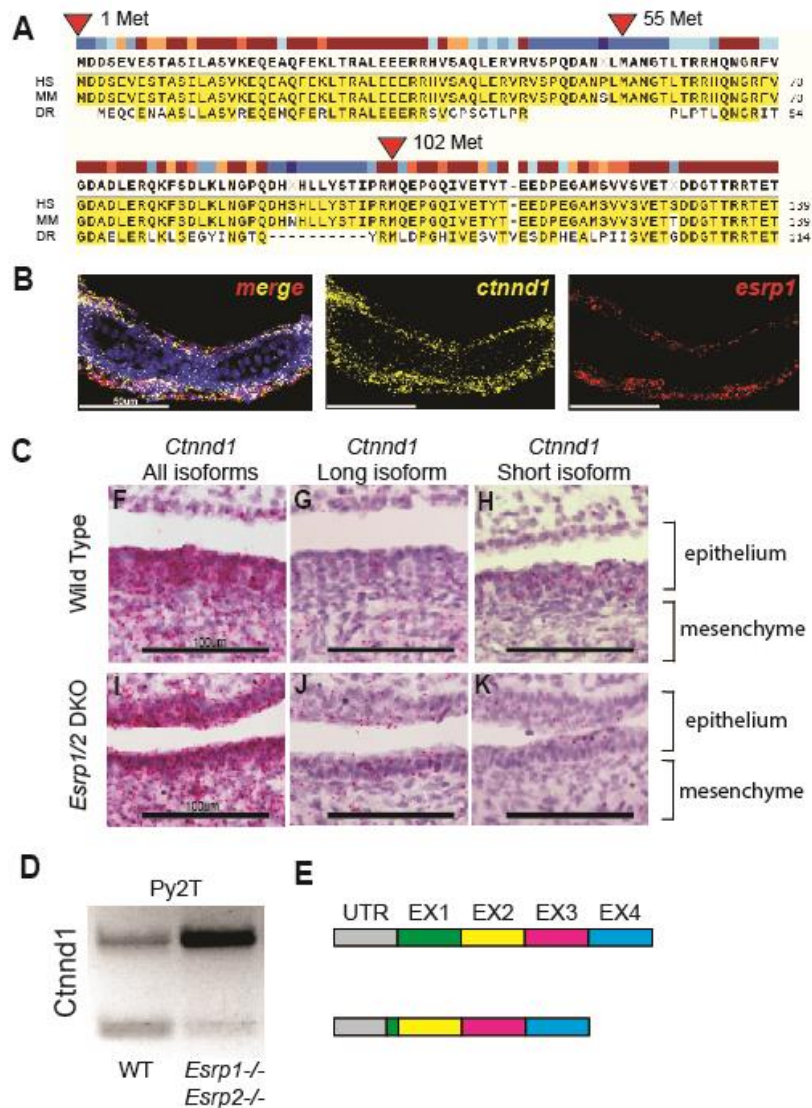
583

584

585

586

## Figure 5



587 **Figure 5. Alternative splicing of *Ctnnd1* is regulated by *Esrp1/2*.** (A) Amino acid sequence  
588 alignment of the first 140 residues of CTNND1 protein across human, mouse, and zebrafish.  
589 Translation for isoform 1 of CTNND1 begins at methionine 1, while isoform 3 encodes a  
590 truncated form that starts translation at methionine 102. Methionine residues at positions 55 and  
591 324 are not conserved across all three species. (B) Detection of *esrp1* and *ctnd1* gene  
592 expression in zebrafish at 4 dpf, demonstrates shared localization of transcripts in the embryonic  
593 epithelium. This coronal section includes the ventral Meckel's cartilage. (C) Detection of murine  
594 *Ctnnd1* mRNA using isoform-specific base-scope probes in the oral epithelium and tongue  
595 mesenchyme. The wildtype sections show that the *Ctnnd1* long isoform is present in both  
596 epithelial and mesenchymal cells. The *Ctnnd1* short isoform is present preferentially in epithelial  
597 cells and not in the mesenchymal cells. In the *Esrp1/2* DKO mouse, the mesenchymal *Ctnnd1*  
598 long isoform is detected in epithelial and mesenchymal cells, with loss of the *Ctnnd1* short  
599 isoform. (D) RT-PCR of the *Ctnnd1* long and short isoforms from Py2T cells. (E) Diagrammatic  
600 representation of the ESERP-regulated *CTNND1* alternative splicing to generate the shorter  
601 epithelial isoform.

## 602 ***CTNND1* gene variants from OFC cohorts**

603 Twenty-four *CTNND1* gene variants have been reported and a growing number of new  
604 variants have been found in ongoing WGS studies of OFC cohorts (19, 26). In a recent  
605 analysis of 759 OFC trios, we identified 15 variants in *CTNND1* with allele frequencies  
606 less than 0.1% in gnomAD (Figure 3 Supplementary Material). Two variants were *de*  
607 *novo* and one was inherited from an affected parent. Pathogenic variants in *CTNND1*  
608 accounted for 0.8% of the cohort. Only 10% of the cohort had a pathogenic variant in  
609 500 genes implicated in OFC that we analyzed, making *CTNND1* the mostly frequently  
610 mutated variant in this cohort (61). In the gene-based burden test, rare variants were  
611 nominally over-transmitted to affected children ( $p=0.06$ ); *de novo* variants are enriched  
612 in *CTNND1* ( $p=0.005$  for loss-of-function *de novo* variants; 0.001 for protein-altering *de*  
613 *novo* variants). Nearly all the missense variants were classified as variants of unknown  
614 significance, indicating that functional testing is critical. In fact, we estimate that  
615 *CTNND1* mutations account for at least 1.5% of CL/P cases. By comparison, *IRF6*  
616 mutations are estimated to be the most common cause of CL/P, accounting for 2% of  
617 cases. Taken together, *CTNND1* stands to be as important as *IRF6* in contributing to  
618 the genetic risk of syndromic and non-syndromic CL/P.

619

## 620 ***Ctnnd1* over-expression rescue *esrp 1*<sup>-/-</sup>; *esrp 2*<sup>-/-</sup> cleft ANC, curled fin and fused** 621 **otolith phenotypes**

622 To functionally assess the relationship between *Esrp* and *Ctnnd1*, we injected the  
623 zebrafish *ctnnd1* isoform-201 (ENSDART00000106048.4) mRNA into *esrp1*<sup>-/-</sup>; *esrp2*<sup>+/-</sup>



624 offspring at the 1-cell stage. Mutants and control embryos were analyzed at 4 dpf,  
625 assessing the ANC, the pectoral fin, and otoliths phenotypes, followed by genotyping  
626 (figure 6A).

627 Control *gfp* mRNA injected *esrp1*<sup>-/-</sup>; *esrp2*<sup>-/-</sup> larvae, exhibited cleft ANC, the  
628 pectoral fins were hypoplastic and stuck to the thorax, and fused otoliths, the mutant  
629 phenotypes were fully penetrant and reliably scored (Figure 6B-E). In the *ctnnd1* mRNA  
630 injected *esrp1*<sup>-/-</sup>; *esrp2*<sup>-/-</sup> larvae, 22% (n = 20 of 90, p<0.01) demonstrated a full or  
631 partial rescue of the ANC (Figure 6B-E). Correspondingly, the injected *esrp1*<sup>-/-</sup>; *esrp2*<sup>-/-</sup>  
632 larvae exhibited significant rescue of the abrogated fin phenotype, with 21% (n = 19 of  
633 90, p<0.01) exhibiting extension of the pectoral fin and angling away from the thorax.  
634 The fused otolith phenotype was scored as either separate or fused, and demonstrated  
635 26% (n = 26 of 90, p<0.01) rescue (Figure 6A). The morphogenesis of the ANC,  
636 pectoral fin and the otoliths all reflect different aspects of embryonic epithelium  
637 development and interaction with the associated mesenchyme of the *esrp 1*<sup>-/-</sup>; *esrp 2*<sup>-/-</sup>  
638 embryos. The *ctnnd1* mRNA over-expression rescuing the epithelial defects in the *esrp*  
639 *1*<sup>-/-</sup>; *esrp 2*<sup>-/-</sup> suggests that a key function of *esrp1/2* in epithelial biology is to regulate  
640 *ctnnd1* function.

641

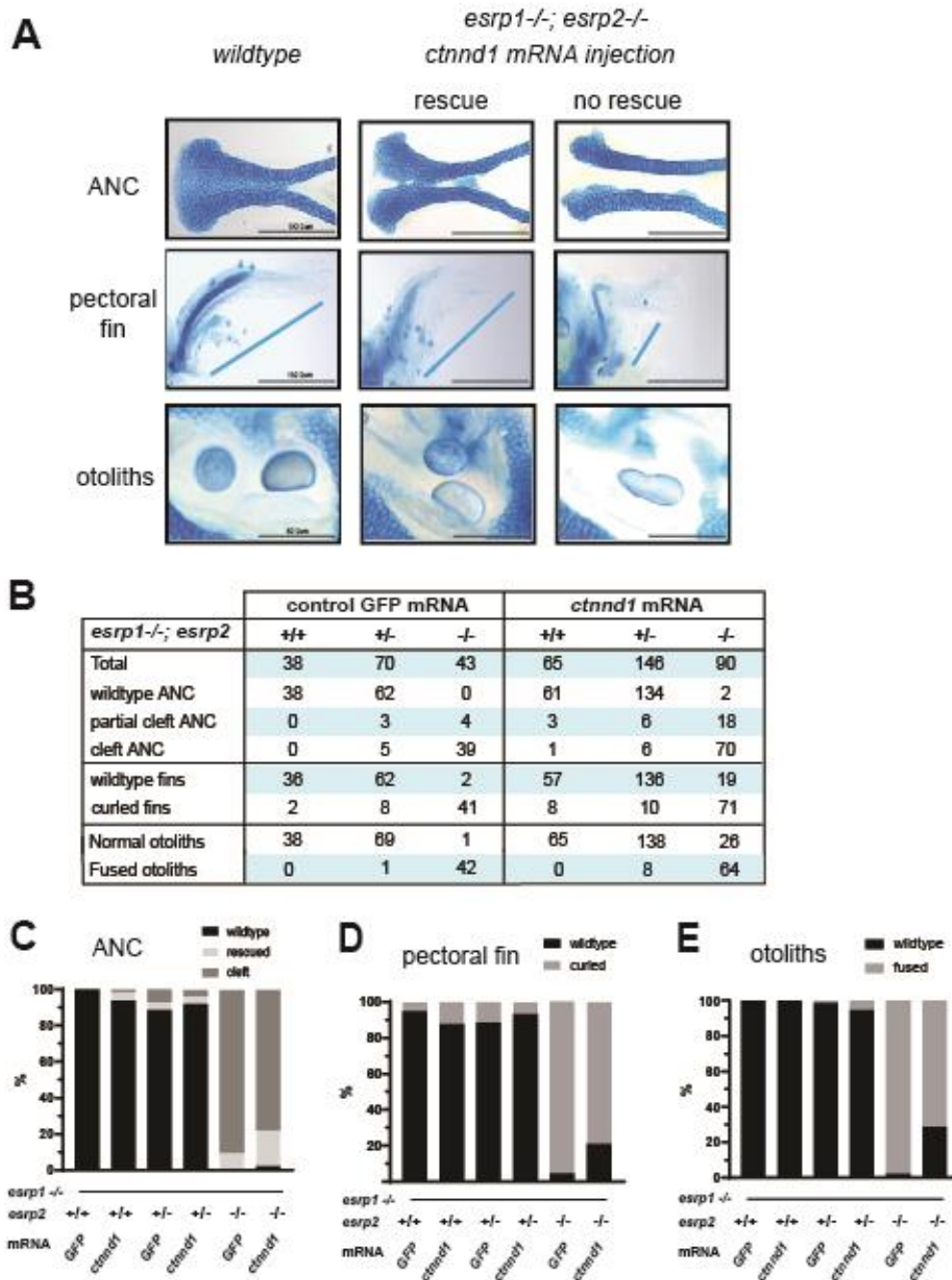
642

643

644

645

## Figure 6



646  
 647 **Figure 6. Over-expression of *ctnd1* rescues *esrp1<sup>-/-</sup>*, *esrp2<sup>-/-</sup>* epithelial phenotypes. (A)**  
 648 Image representing how wild type, intermediate and cleft ANC, pectoral fins and otoliths were  
 649 sorted. (B) Representative table with the number of total fish injected and rescued by the *ctnd1*  
 650 mRNA injection with GFP mRNA injection as control. Scoring of ANC phenotype (%) (C), fin  
 651 phenotype (%) (D) and the otolith phenotype (%) (E) in the injected *esrp1<sup>-/-</sup>; esrp2<sup>+/-</sup>* inter-cross  
 652 larvae confirmed by genotyping, showing 20-22% rescue of ANC, fin and otolith phenotypes in  
 653 the *esrp1<sup>-/-</sup>; esrp2<sup>-/-</sup>* double homozygous larvae.

## 654 Discussion

655 Several independent lines of evidence corroborate that the *ESRP1* and *ESRP2* genes  
656 are important OFC loci in humans. *ESRP1* was proposed to be the most likely  
657 candidate CL/P risk gene in the 8q22.1 locus (83, 84). Ectopic expression of p63  
658 converted human fibroblasts to keratinocyte-like cells and *ESRP1* was transcriptionally  
659 induced together with activation of an epithelial enhancer within a topologically  
660 associated domains (TADs) containing a non-syndromic CL/P risk locus (85). This is  
661 consistent with the biological observation and *p63*, *Irf6* and *Esrp1/2* co-localize in the  
662 embryonic epithelium, and that mutations of these 3 genes result in OFC phenotypes.  
663 Further, a whole exome sequencing study of non-syndromic CL/P in multi-affected  
664 families identified pathogenic variants in *ESRP2* with an autosomal dominant  
665 inheritance pattern (20).

666 Several studies showed in mouse and zebrafish models that *Esrp1* and *Esrp2*  
667 are important in craniofacial development. We showed that *Esrp1* and *Esrp2* are co-  
668 localized with *Irf6* in the embryonic oral epithelium, and when *Esrp1/2* are disrupted,  
669 cleft of the lip and palate formed, validating that mouse and zebrafish are robust animal  
670 models of human OFC (21, 52, 53).

671 There is growing recognition that RNA binding proteins that regulate alternative  
672 splicing play vital roles in craniofacial morphogenesis. Clinically, spliceosomopathies  
673 are often associated with syndromic craniofacial abnormalities due to disruption of  
674 splicing factors such as *PUF60*, *ETUD2*, *SF3B4*, *RBM10*, and *ESRP2* (86). Animal  
675 models defective in RNA splicing that exhibit craniofacial phenotypes include: *Esrp1/2*,  
676 *Rbfox2*, *Srsf3*, and *Sf3b2* (21, 22, 52, 87, 88). The ESRP proteins are uniquely

677 expressed in epithelial structures and direct post-transcriptional modifications that  
678 distinguish protein isoforms between epithelium and mesenchyme. We applied  
679 complementary phenotypic and molecular assays to interrogate the functional  
680 consequence of identified *ESRP1/2* gene variants in cohorts of autosomal recessive  
681 deafness and CL/P.

682         As the magnitude of available WGS data increases, the need for assigning  
683 clinically actionable information continues to grow. The sequence variant interpretation  
684 (SVI) working group from ACMG-AMP frequently reconvenes to update, revise, and  
685 refine the ACMG criteria to provide the clearest guidance possible (33, 34). Most  
686 recently, the working group provided further guidance regarding functional assays and  
687 experimental model systems. Among these, they highlighted the need to ascertain the  
688 gene variants' physiologic context and molecular consequence. Here, we applied  
689 complementary phenotypic assays in the zebrafish ANC rescue, in addition to the Py2T  
690 splicing assay, to assess the physiologic and molecular consequences of *ESRP1/2*  
691 gene variants observed in clinical cohorts. These functional tests identified 7 pathogenic  
692 variants out of 18 *ESRP1/2* variants examined. Moreover, these functional readouts of  
693 orthologous systems across species attest to the strongly conserved nature of epithelial  
694 splicing by the *ESRPs* in craniofacial morphogenesis. These results highlight the need  
695 for experimental models to enhance the validity of *in silico* predictions of protein  
696 function. We found that while the SIFT and PolyPhen-2 algorithms have a positive  
697 predictive value when they align in predicting benign variants, they tend to overestimate  
698 the prevalence of pathogenic variants.

699           While AlphaMissense provided slightly better predictions for *ESRP1* than SIFT  
700   and PolyPhen-2, in the case of *ESRP2*, AlphaMissense over-interpreted benign variants  
701   as pathogenic. A similar high false positive rate was seen in a different disease, cystic  
702   fibrosis transmembrane conductance regulator (89), and for epithelial master regulator  
703   *IRF6* (90). This work highlights that protein structure and machine learning approaches  
704   today are still insufficient to accurately predict pathogenicity, where functional tests are  
705   indispensable to validate the pathogenicity of variants.

706           These functional assays revealed novel insights into *ESRP1/2* protein function  
707   and downstream targets spliced by the *ESRPs*. We found that the gene variants with  
708   the largest effect size for the zebrafish ANC rescue assay lie in RRM1 and RRM3 of  
709   *ESRP2*. Variants R250Q and R353Q were predicted by PolyPhen-2, SIFT and  
710   AlphaMissense to be damaging or likely pathogenic, but in both independent functional  
711   tests corroborated to be benign variants. In contrast, R315H was functionally tested by  
712   both assays to be a deleterious variant, consistent with prior work demonstrating R315  
713   to impact RNA binding based on protein structure analysis (91). Furthermore, we  
714   provide molecular evidence that *Esrp* transcripts rescue molecular splicing patterns of  
715   putative *Esrp*-target genes *Arhgef11* and *Ctnnd1*. Moreover, gene variants with  
716   pathogenic potential do not restore splicing patterns of *Arhgef11*, providing evidence  
717   that the gene variants impair *Esrp* function and likely contribute to disease  
718   pathogenicity. These functional assays provide key data to satisfy the ACMG-AMP  
719   standards, where molecular assays are used to contribute to our understanding of  
720   mechanisms for disease.

721 Mutations in *CTNND1* and *CDH1* (E-cadherin) are the known cause of BCD,  
722 which includes abnormal eyelids, upper lip, palate, and teeth development (20, 74, 92).  
723 The precise pathological mechanism remains to be elucidated, but in healthy epithelial  
724 cells *CTNND1* binds to E-cadherin to stabilize adherens junctions and desmosomes,  
725 and therefore displacement of *CTNND1* causes endocytosis of *CDH1* and loss of the  
726 junction. Another possibility is disruption of the canonical WNT pathway signaling, as  
727 *CTNND1* is known to modulate transcription by binding to transcription factors such as  
728 Kaiso in the *Wnt* pathway (93, 94). It is known, and further supported by the evidence in  
729 this work, that alternatively spliced isoforms of *CTNND1* are differentially expressed in  
730 the epithelium and mesenchyme, and here we show that those distinct splicing patterns  
731 are dependent on *Esrp1/2* activity. However, it is not known how the alternatively  
732 spliced isoforms differ in function, alter embryonic and craniofacial morphogenesis, or  
733 contribute to disease. Thus, further studies into the functional differences between  
734 *CTNND1* isoforms are warranted and would provide insight into the disease etiology of  
735 BCD or the mechanism of the cleft palate from *ESRP* loss-of-function.

736 **Acknowledgements**

737 We thank the Aquatics Core at Massachusetts General Hospital and Children's Hospital  
738 of Philadelphia (CHOP) for their dedication to fish health and maintenance of our  
739 colonies. We thank the CHOP IDDRC Biostatistics and Data Science core (HD105354)  
740 for consultation. We are grateful for the funding support from the National Institutes of  
741 Health (HG013031) to K.W. and (DE032332, DE027983) to E.C.L., research and  
742 fellowship grants from Shriners Hospitals for Children and institutional support from  
743 Children's Hospital of Philadelphia.

744

## 745 References

- 746
- 747 1. Bishop MR, Diaz Perez KK, Sun M, Ho S, Chopra P, Mukhopadhyay N, et al. Genome-wide  
748 Enrichment of De Novo Coding Mutations in Orofacial Cleft Trios. *Am J Hum Genet.* 2020;107(1):124-36.
  - 749 2. Bureau A, Parker MM, Ruczinski I, Taub MA, Marazita ML, Murray JC, et al. Whole exome  
750 sequencing of distant relatives in multiplex families implicates rare variants in candidate genes for oral  
751 clefts. *Genetics.* 2014;197(3):1039-44.
  - 752 3. Carlson JC, Taub MA, Feingold E, Beaty TH, Murray JC, Marazita ML, et al. Identifying Genetic  
753 Sources of Phenotypic Heterogeneity in Orofacial Clefts by Targeted Sequencing. *Birth Defects Res.*  
754 2017;109(13):1030-8.
  - 755 4. Leslie EJ. Genetic models and approaches to study orofacial clefts. *Oral Dis.* 2021.
  - 756 5. Mukhopadhyay N, Feingold E, Moreno-Urbe L, Wehby G, Valencia-Ramirez LC, Muneton CPR, et  
757 al. Genome-Wide Association Study of Non-syndromic Orofacial Clefts in a Multiethnic Sample of  
758 Families and Controls Identifies Novel Regions. *Front Cell Dev Biol.* 2021;9:621482.
  - 759 6. Beaty TH, Marazita ML, Leslie EJ. Genetic factors influencing risk to orofacial clefts: today's  
760 challenges and tomorrow's opportunities. *F1000Res.* 2016;5:2800.
  - 761 7. Dixon MJ, Marazita ML, Beaty TH, Murray JC. Cleft lip and palate: understanding genetic and  
762 environmental influences. *Nat Rev Genet.* 2011;12(3):167-78.
  - 763 8. Welzenbach J, Hammond NL, Nikolic M, Thieme F, Ishorst N, Leslie EJ, et al. Integrative  
764 approaches generate insights into the architecture of non-syndromic cleft lip with or without cleft  
765 palate. *HGG Adv.* 2021;2(3):100038.
  - 766 9. Carlson JC, Anand D, Butali A, Buxo CJ, Christensen K, Deleyiannis F, et al. A systematic genetic  
767 analysis and visualization of phenotypic heterogeneity among orofacial cleft GWAS signals. *Genet*  
768 *Epidemiol.* 2019;43(6):704-16.
  - 769 10. Curtis SW, Chang D, Lee MK, Shaffer JR, Indencleef K, Epstein MP, et al. The PAX1 locus at 20p11  
770 is a potential genetic modifier for bilateral cleft lip. *HGG Adv.* 2021;2(2).
  - 771 11. Takahashi M, Hosomichi K, Yamaguchi T, Nagahama R, Yoshida H, Maki K, et al. Whole-genome  
772 sequencing in a pair of monozygotic twins with discordant cleft lip and palate subtypes. *Oral Dis.*  
773 2018;24(7):1303-9.
  - 774 12. Richardson R, Mitchell K, Hammond NL, Mollo MR, Kouwenhoven EN, Wyatt ND, et al. p63  
775 exerts spatio-temporal control of palatal epithelial cell fate to prevent cleft palate. *PLoS Genet.*  
776 2017;13(6):e1006828.
  - 777 13. Ferretti E, Li B, Zewdu R, Wells V, Hebert JM, Karner C, et al. A conserved Pbx-Wnt-p63-Irf6  
778 regulatory module controls face morphogenesis by promoting epithelial apoptosis. *Developmental cell.*  
779 2011;21(4):627-41.
  - 780 14. Kondo S, Schutte BC, Richardson RJ, Bjork BC, Knight AS, Watanabe Y, et al. Mutations in IRF6  
781 cause Van der Woude and popliteal pterygium syndromes. *Nat Genet.* 2002;32(2):285-9.
  - 782 15. Ingraham CR, Kinoshita A, Kondo S, Yang B, Sajan S, Trout KJ, et al. Abnormal skin, limb and  
783 craniofacial morphogenesis in mice deficient for interferon regulatory factor 6 (Irf6). *Nat Genet.*  
784 2006;38(11):1335-40.
  - 785 16. Richardson RJ, Dixon J, Malhotra S, Hardman MJ, Knowles L, Boot-Handford RP, et al. Irf6 is a key  
786 determinant of the keratinocyte proliferation-differentiation switch. *Nat Genet.* 2006;38(11):1329-34.
  - 787 17. de la Garza G, Schleiffarth JR, Dunnwald M, Mankad A, Weirather JL, Bonde G, et al. Interferon  
788 regulatory factor 6 promotes differentiation of the periderm by activating expression of Grainyhead-like  
789 3. *J Invest Dermatol.* 2013;133(1):68-77.
  - 790 18. Peyrard-Janvid M, Leslie EJ, Kousa YA, Smith TL, Dunnwald M, Magnusson M, et al. Dominant  
791 mutations in GRHL3 cause Van der Woude Syndrome and disrupt oral periderm development. *Am J Hum*  
792 *Genet.* 2014;94(1):23-32.



- 793 19. Alharatani R, Ververi A, Beleza-Meireles A, Ji W, Mis E, Patterson QT, et al. Novel truncating  
794 mutations in CTNND1 cause a dominant craniofacial and cardiac syndrome. *Hum Mol Genet.*  
795 2020;29(11):1900-21.
- 796 20. Cox LL, Cox TC, Moreno Uribe LM, Zhu Y, Richter CT, Nidey N, et al. Mutations in the Epithelial  
797 Cadherin-p120-Catenin Complex Cause Mendelian Non-Syndromic Cleft Lip with or without Cleft Palate.  
798 *Am J Hum Genet.* 2018;102(6):1143-57.
- 799 21. Bebee TW, Park JW, Sheridan KI, Warzecha CC, Cieply BW, Rohacek AM, et al. The splicing  
800 regulators *Esrp1* and *Esrp2* direct an epithelial splicing program essential for mammalian development.  
801 *Elife.* 2015;4.
- 802 22. Burguera D, Marquez Y, Racioppi C, Permanyer J, Torres-Mendez A, Esposito R, et al.  
803 Evolutionary recruitment of flexible *Esrp*-dependent splicing programs into diverse embryonic  
804 morphogenetic processes. *Nat Commun.* 2017;8(1):1799.
- 805 23. Lee S, Cieply B, Yang Y, Peart N, Glaser C, Chan P, et al. *Esrp1*-Regulated Splicing of *Arhgef11*  
806 Isoforms Is Required for Epithelial Tight Junction Integrity. *Cell Rep.* 2018;25(9):2417-30 e5.
- 807 24. Yang Y, Carstens RP. Alternative splicing regulates distinct subcellular localization of Epithelial  
808 splicing regulatory protein 1 (*Esrp1*) isoforms. *Sci Rep.* 2017;7(1):3848.
- 809 25. Adzhubei IA, Schmidt S, Peshkin L, Ramensky VE, Gerasimova A, Bork P, et al. A method and  
810 server for predicting damaging missense mutations. *Nat Methods.* 2010;7(4):248-9.
- 811 26. Choi Y, Sims GE, Murphy S, Miller JR, Chan AP. Predicting the functional effect of amino acid  
812 substitutions and indels. *PLoS One.* 2012;7(10):e46688.
- 813 27. Kumar P, Henikoff S, Ng PC. Predicting the effects of coding non-synonymous variants on protein  
814 function using the SIFT algorithm. *Nat Protoc.* 2009;4(7):1073-81.
- 815 28. Reva B, Antipin Y, Sander C. Predicting the functional impact of protein mutations: application to  
816 cancer genomics. *Nucleic Acids Res.* 2011;39(17):e118.
- 817 29. Tang H, Thomas PD. Tools for Predicting the Functional Impact of Nonsynonymous Genetic  
818 Variation. *Genetics.* 2016;203(2):635-47.
- 819 30. Liu X, Li C, Mou C, Dong Y, Tu Y. dbNSFP v4: a comprehensive database of transcript-specific  
820 functional predictions and annotations for human nonsynonymous and splice-site SNVs. *Genome Med.*  
821 2020;12(1):103.
- 822 31. Frazer J, Notin P, Dias M, Gomez A, Min JK, Brock K, et al. Disease variant prediction with deep  
823 generative models of evolutionary data. *Nature.* 2021;599(7883):91-5.
- 824 32. Oliver JD, Turner EC, Halpern LR, Jia S, Schneider P, D'Souza RN. Molecular Diagnostics and In  
825 Utero Therapeutics for Orofacial Clefts. *J Dent Res.* 2020;99(11):1221-7.
- 826 33. Richards S, Aziz N, Bale S, Bick D, Das S, Gastier-Foster J, et al. Standards and guidelines for the  
827 interpretation of sequence variants: a joint consensus recommendation of the American College of  
828 Medical Genetics and Genomics and the Association for Molecular Pathology. *Genet Med.*  
829 2015;17(5):405-24.
- 830 34. Bean LJH, Funke B, Carlston CM, Gannon JL, Kantarci S, Krock BL, et al. Diagnostic gene  
831 sequencing panels: from design to report—a technical standard of the American College of Medical  
832 Genetics and Genomics (ACMG). *Genet Med.* 2020;22(3):453-61.
- 833 35. Jaravine V, Balmford J, Metzger P, Boerries M, Binder H, Boeker M. Annotation of Human Exome  
834 Gene Variants with Consensus Pathogenicity. *Genes (Basel).* 2020;11(9).
- 835 36. Harnish JM, Deal SL, Chao HT, Wangler MF, Yamamoto S. In Vivo Functional Study of Disease-  
836 associated Rare Human Variants Using *Drosophila*. *J Vis Exp.* 2019(150).
- 837 37. Wang J, Liu Z, Bellen HJ, Yamamoto S. Navigating MARRVEL, a Web-Based Tool that Integrates  
838 Human Genomics and Model Organism Genetics Information. *J Vis Exp.* 2019(150).

- 839 38. Raud L, Ka C, Gourlaouen I, Callebaut I, Ferec C, Le Gac G, et al. Functional analysis of novel RHD  
840 variants: splicing disruption is likely to be a common mechanism of variant D phenotype. *Transfusion*.  
841 2019;59(4):1367-75.
- 842 39. Schaid DJ, Chen W, Larson NB. From genome-wide associations to candidate causal variants by  
843 statistical fine-mapping. *Nat Rev Genet*. 2018;19(8):491-504.
- 844 40. Li EB, Truong D, Hallett SA, Mukherjee K, Schutte BC, Liao EC. Rapid functional analysis of  
845 computationally complex rare human IRF6 gene variants using a novel zebrafish model. *PLoS Genet*.  
846 2017;13(9):e1007009.
- 847 41. Kim SS, Dey KK, Weissbrod O, Marquez-Luna C, Gazal S, Price AL. Improving the informativeness  
848 of Mendelian disease-derived pathogenicity scores for common disease. *Nat Commun*. 2020;11(1):6258.
- 849 42. Itan Y, Shang L, Boisson B, Ciancanelli MJ, Markle JG, Martinez-Barricarte R, et al. The mutation  
850 significance cutoff: gene-level thresholds for variant predictions. *Nat Methods*. 2016;13(2):109-10.
- 851 43. Liu Y, Yeung WSB, Chiu PCN, Cao D. Computational approaches for predicting variant impact: An  
852 overview from resources, principles to applications. *Front Genet*. 2022;13:981005.
- 853 44. Zhang M, Zhang J, Zhao H, Ievlev V, Zhong W, Huang W, et al. Functional Characterization of a  
854 Novel IRF6 Frameshift Mutation From a Van Der Woude Syndrome Family. *Front Genet*. 2020;11:562.
- 855 45. Griesemer D, Xue JR, Reilly SK, Ulirsch JC, Kukreja K, Davis JR, et al. Genome-wide functional  
856 screen of 3'UTR variants uncovers causal variants for human disease and evolution. *Cell*.  
857 2021;184(20):5247-60 e19.
- 858 46. Findlay GM, Daza RM, Martin B, Zhang MD, Leith AP, Gasperini M, et al. Accurate classification  
859 of BRCA1 variants with saturation genome editing. *Nature*. 2018;562(7726):217-22.
- 860 47. Glazer AM, Wada Y, Li B, Muhammad A, Kalash OR, O'Neill MJ, et al. High-Throughput  
861 Reclassification of SCN5A Variants. *Am J Hum Genet*. 2020;107(1):111-23.
- 862 48. Giacomelli AO, Yang X, Lintner RE, McFarland JM, Duby M, Kim J, et al. Mutational processes  
863 shape the landscape of TP53 mutations in human cancer. *Nat Genet*. 2018;50(10):1381-7.
- 864 49. Mighell TL, Evans-Dutson S, O'Roak BJ. A Saturation Mutagenesis Approach to Understanding  
865 PTEN Lipid Phosphatase Activity and Genotype-Phenotype Relationships. *Am J Hum Genet*.  
866 2018;102(5):943-55.
- 867 50. Jia X, Burugula BB, Chen V, Lemons RM, Jayakody S, Maksutova M, et al. Massively parallel  
868 functional testing of MSH2 missense variants conferring Lynch syndrome risk. *Am J Hum Genet*.  
869 2021;108(1):163-75.
- 870 51. Warzecha CC, Sato TK, Nabet B, Hogenesch JB, Carstens RP. ESRP1 and ESRP2 are epithelial cell-  
871 type-specific regulators of FGFR2 splicing. *Mol Cell*. 2009;33(5):591-601.
- 872 52. Carroll SH, Macias Trevino C, Li EB, Kawasaki K, Myers N, Hallett SA, et al. An Irf6-Esrp1/2  
873 regulatory axis controls midface morphogenesis in vertebrates. *Development*. 2020;147(24).
- 874 53. Lee S, Sears MJ, Zhang Z, Li H, Salhab I, Krebs P, et al. Cleft lip and cleft palate in *Esrp1* knockout  
875 mice is associated with alterations in epithelial-mesenchymal crosstalk. *Development*. 2020;147(21).
- 876 54. Schilling TF, Kimmel CB. Musculoskeletal patterning in the pharyngeal segments of the zebrafish  
877 embryo. *Development*. 1997;124(15):2945-60.
- 878 55. Wada N, Javidan Y, Nelson S, Carney TJ, Kelsh RN, Schilling TF. Hedgehog signaling is required for  
879 cranial neural crest morphogenesis and chondrogenesis at the midline in the zebrafish skull.  
880 *Development*. 2005;132(17):3977-88.
- 881 56. Dougherty M, Kamel G, Grimaldi M, Gfrerer L, Shubinets V, Ethier R, et al. Distinct requirements  
882 for *wnt9a* and *irf6* in extension and integration mechanisms during zebrafish palate morphogenesis.  
883 *Development*. 2013;140(1):76-81.
- 884 57. Swartz ME, Sheehan-Rooney K, Dixon MJ, Eberhart JK. Examination of a palatogenic gene  
885 program in zebrafish. *Dev Dyn*. 2011;240(9):2204-20.

- 886 58. Rohacek AM, Bebee TW, Tilton RK, Radens CM, McDermott-Roe C, Peart N, et al. ESRP1  
887 Mutations Cause Hearing Loss due to Defects in Alternative Splicing that Disrupt Cochlear Development.  
888 *Dev Cell*. 2017;43(3):318-31 e5.
- 889 59. Freytag M, Kluth M, Bady E, Hube-Magg C, Makrypidi-Fraune G, Heinzer H, et al. Epithelial  
890 splicing regulatory protein 1 and 2 (ESRP1 and ESRP2) upregulation predicts poor prognosis in prostate  
891 cancer. *BMC Cancer*. 2020;20(1):1220.
- 892 60. Peart NJ, Hwang JY, Quesnel-Vallieres M, Sears MJ, Yang Y, Stoilov P, et al. The global Protein-  
893 RNA interaction map of ESRP1 defines a post-transcriptional program that is essential for epithelial cell  
894 function. *iScience*. 2022;25(10):105205.
- 895 61. Diaz Perez KK, Curtis SW, Sanchis-Juan A, Zhao X, Head T, Ho S, et al. Rare variants found in  
896 clinical gene panels illuminate the genetic and allelic architecture of orofacial clefting. *Genet Med*.  
897 2023;25(10):100918.
- 898 62. Sievers F, Higgins DG. The Clustal Omega Multiple Alignment Package. *Methods Mol Biol*.  
899 2021;2231:3-16.
- 900 63. Samocha KE, Robinson EB, Sanders SJ, Stevens C, Sabo A, McGrath LM, et al. A framework for  
901 the interpretation of de novo mutation in human disease. *Nat Genet*. 2014;46(9):944-50.
- 902 64. Walker MB, Kimmel CB. A two-color acid-free cartilage and bone stain for zebrafish larvae.  
903 *Biotech Histochem*. 2007;82(1):23-8.
- 904 65. Panizzi JR, Jessen JR, Drummond IA, Solnica-Krezel L. New functions for a vertebrate Rho  
905 guanine nucleotide exchange factor in ciliated epithelia. *Development*. 2007;134(5):921-31.
- 906 66. Warzecha CC, Shen S, Xing Y, Carstens RP. The epithelial splicing factors ESRP1 and ESRP2  
907 positively and negatively regulate diverse types of alternative splicing events. *RNA Biol*. 2009;6(5):546-  
908 62.
- 909 67. Itoh M, Radisky DC, Hashiguchi M, Sugimoto H. The exon 38-containing ARHGEF11 splice  
910 isoform is differentially expressed and is required for migration and growth in invasive breast cancer  
911 cells. *Oncotarget*. 2017;8(54):92157-70.
- 912 68. Shapiro IM, Cheng AW, Flytzanis NC, Balsamo M, Condeelis JS, Oktay MH, et al. An EMT-driven  
913 alternative splicing program occurs in human breast cancer and modulates cellular phenotype. *PLoS*  
914 *Genet*. 2011;7(8):e1002218.
- 915 69. Landrum MJ, Chitipiralla S, Brown GR, Chen C, Gu B, Hart J, et al. ClinVar: improvements to  
916 accessing data. *Nucleic Acids Res*. 2020;48(D1):D835-D44.
- 917 70. Sayers EW, Beck J, Bolton EE, Bourexis D, Brister JR, Canese K, et al. Database resources of the  
918 National Center for Biotechnology Information. *Nucleic Acids Res*. 2021;49(D1):D10-D7.
- 919 71. Mukhopadhyay N, Bishop M, Mortillo M, Chopra P, Hetmanski JB, Taub MA, et al. Whole  
920 genome sequencing of orofacial cleft trios from the Gabriella Miller Kids First Pediatric Research  
921 Consortium identifies a new locus on chromosome 21. *Hum Genet*. 2020;139(2):215-26.
- 922 72. Cheng J, Novati G, Pan J, Bycroft C, Zemgulyte A, Applebaum T, et al. Accurate proteome-wide  
923 missense variant effect prediction with AlphaMissense. *Science*. 2023;381(6664):eadg7492.
- 924 73. Faux MC, King LE, Kane SR, Love C, Sieber OM, Burgess AW. APC regulation of ESRP1 and p120-  
925 catenin isoforms in colorectal cancer cells. *Mol Biol Cell*. 2021;32(2):120-30.
- 926 74. Kievit A, Tessadori F, Douben H, Jordens I, Maurice M, Hoogeboom J, et al. Variants in members  
927 of the cadherin-catenin complex, CDH1 and CTNND1, cause blepharocheilodontic syndrome. *Eur J Hum*  
928 *Genet*. 2018;26(2):210-9.
- 929 75. Davis MA, Ireton RC, Reynolds AB. A core function for p120-catenin in cadherin turnover. *J Cell*  
930 *Biol*. 2003;163(3):525-34.
- 931 76. Fukumoto Y, Shintani Y, Reynolds AB, Johnson KR, Wheelock MJ. The regulatory or  
932 phosphorylation domain of p120 catenin controls E-cadherin dynamics at the plasma membrane. *Exp*  
933 *Cell Res*. 2008;314(1):52-67.

- 934 77. Ireton RC, Davis MA, van Hengel J, Mariner DJ, Barnes K, Thoreson MA, et al. A novel role for  
935 p120 catenin in E-cadherin function. *J Cell Biol.* 2002;159(3):465-76.
- 936 78. Ishiyama N, Lee SH, Liu S, Li GY, Smith MJ, Reichardt LF, et al. Dynamic and static interactions  
937 between p120 catenin and E-cadherin regulate the stability of cell-cell adhesion. *Cell.* 2010;141(1):117-  
938 28.
- 939 79. Reynolds AB, Daniel J, McCrean PD, Wheelock MJ, Wu J, Zhang Z. Identification of a new catenin:  
940 the tyrosine kinase substrate p120cas associates with E-cadherin complexes. *Mol Cell Biol.*  
941 1994;14(12):8333-42.
- 942 80. Reynolds AB, Daniel JM, Mo YY, Wu J, Zhang Z. The novel catenin p120cas binds classical  
943 cadherins and induces an unusual morphological phenotype in NIH3T3 fibroblasts. *Exp Cell Res.*  
944 1996;225(2):328-37.
- 945 81. Schackmann RC, Tenhagen M, van de Ven RA, Derksen PW. p120-catenin in cancer -  
946 mechanisms, models and opportunities for intervention. *J Cell Sci.* 2013;126(Pt 16):3515-25.
- 947 82. Stairs DB, Bayne LJ, Rhoades B, Vega ME, Waldron TJ, Kalabis J, et al. Deletion of p120-catenin  
948 results in a tumor microenvironment with inflammation and cancer that establishes it as a tumor  
949 suppressor gene. *Cancer Cell.* 2011;19(4):470-83.
- 950 83. Overhoff J, Rabideau MM, Bird LM, Schweitzer DN, Haynes K, Schultz RA, et al. Refinement of  
951 the 8q22.1 microdeletion critical region associated with Nablus mask-like facial syndrome. *Am J Med*  
952 *Genet A.* 2014;164A(1):259-63.
- 953 84. Yu Y, Zuo X, He M, Gao J, Fu Y, Qin C, et al. Genome-wide analyses of non-syndromic cleft lip  
954 with palate identify 14 novel loci and genetic heterogeneity. *Nat Commun.* 2017;8:14364.
- 955 85. Lin-Shiao E, Lan Y, Welzenbach J, Alexander KA, Zhang Z, Knapp M, et al. p63 establishes  
956 epithelial enhancers at critical craniofacial development genes. *Sci Adv.* 2019;5(5):eaaw0946.
- 957 86. Griffin C, Saint-Jeannet JP. Spliceosomopathies: Diseases and mechanisms. *Dev Dyn.*  
958 2020;249(9):1038-46.
- 959 87. Dennison BJC, Larson ED, Fu R, Mo J, Fantauzzo KA. Srsf3 mediates alternative RNA splicing  
960 downstream of PDGFRalpha signaling in the facial mesenchyme. *Development.* 2021;148(14).
- 961 88. Timberlake AT, Griffin C, Heike CL, Hing AV, Cunningham ML, Chitayat D, et al. Haploinsufficiency  
962 of SF3B2 causes craniofacial microsomia. *Nat Commun.* 2021;12(1):4680.
- 963 89. Eli Fritz McDonald KEO, Jonathan P. Schleich, Jens Meiler, Lars Plate. Pre-print Benchmarking  
964 AlphaMissense Pathogenicity Predictions Against Cystic Fibrosis Variants BioRxiv. 2023.
- 965 90. Murali H, Wang P, Liao EC, Wang K. Genetic variant classification by predicted protein structure:  
966 A case study on IRF6. *Comput Struct Biotechnol J.* 2024;23:892-904.
- 967 91. Dominguez C, Fiset JF, Chabot B, Allain FH. Structural basis of G-tract recognition and engaging  
968 by hnRNP F quasi-RRMs. *Nat Struct Mol Biol.* 2010;17(7):853-61.
- 969 92. Ghomid J, Stichelbout M, Jourdain AS, Frenois F, Lejeune-Dumoulin S, Alex-Cordier MP, et al.  
970 Blepharochelodontic syndrome is a CDH1 pathway-related disorder due to mutations in CDH1 and  
971 CTNND1. *Genet Med.* 2017;19(9):1013-21.
- 972 93. Del Valle-Perez B, Casagolda D, Lugalde E, Valls G, Codina M, Dave N, et al. Wnt controls the  
973 transcriptional activity of Kaiso through CK1epsilon-dependent phosphorylation of p120-catenin. *J Cell*  
974 *Sci.* 2011;124(Pt 13):2298-309.
- 975 94. Park JI, Kim SW, Lyons JP, Ji H, Nguyen TT, Cho K, et al. Kaiso/p120-catenin and TCF/beta-catenin  
976 complexes coordinately regulate canonical Wnt gene targets. *Developmental cell.* 2005;8(6):843-54.

977